Physiol Genomics 24: 198–206, 2006.
First published December 20, 2005; doi:10.1152/physiolgenomics.00221.2005.

TRANSLATIONAL PHYSIOLOGY

WTC deafness Kyoto (*dfk*): a rat model for extensive investigations of *Kcnq1* functions

Hiroshi Gohma,[1] Takashi Kuramoto,[1] Mitsuru Kuwamura,[2] Ryoko Okajima,[2] Noriaki Tanimoto,[3] Ken-ichi Yamasaki,[1] Satoshi Nakanishi,[1] Kazuhiro Kitada,[1] Takeru Makiyama,[4] Masaharu Akao,[4] Toru Kita,[4] Masashi Sasa,[5] and Tadao Serikawa[1]

[1]*Institute of Laboratory Animals, Graduate School of Medicine, Kyoto University, Kyoto, Japan;* [2]*Laboratory of Veterinary Pathology, Osaka Prefecture University, Sakai, Japan;* [3]*Safety Research Laboratory, Tanabe Seiyaku Company, Limited, Osaka, Japan;* [4]*Department of Cardiovascular Medicine, Graduate School of Medicine, Kyoto University, Kyoto, Japan; and* [5]*Nagisa Hospital, Hirakata, Japan*

Submitted 13 August 2005; accepted in final form 7 December 2005

Gohma, Hiroshi, Takashi Kuramoto, Mitsuru Kuwamura, Ryoko Okajima, Noriaki Tanimoto, Ken-ichi Yamasaki, Satoshi Nakanishi, Kazuhiro Kitada, Takeru Makiyama, Masaharu Akao, Toru Kita, Masashi Sasa, and Tadao Serikawa. WTC deafness Kyoto (*dfk*): a rat model for extensive investigations of *Kcnq1* functions. *Physiol Genomics* 24: 198–206, 2006. First published December 20, 2005; doi:10.1152/physiolgenomics.00221.2005.—KCNQ1 forms K^+ channels by assembly with regulatory subunit KCNE proteins and plays a key role in the K^+ homeostasis in a variety of tissues. In the heart, KCNQ1 is coassembled with KCNE1 to produce a cardiac delayed rectifier K^+ current. In the inner ear, the KCNQ1/KCNE1 complex maintains the high concentration of K^+ in the endolymph. In the stomach, KCNQ1 is coassembled with KCNE2 to form the K^+ exflux channel that is essential for gastric acid secretion. In the colon and small intestine, KCNQ1 is coassembled with KCNE3 to play an important role in transepithelial cAMP-stimulated Cl^- secretion. For further understanding of *Kcnq1* function in vivo, an animal model has been required. Here we reported the identification of a coisogenic *Kcnq1* mutant rat, named deafness Kyoto (*dfk*), and the characterization of its phenotypes. WTC-*dfk* rats carried intragenic deletion at the *Kcnq1* gene and showed impaired gain of weight, deafness, and imbalance resulting from the marked reduction of endolymph, prolonged QT interval in the electrocardiogram (ECG), and gastric achlorhydria associated with hypertrophic gastric mucosa. Surprisingly, WTC-*dfk* rats showed hypertension, which suggested that *Kcnq1* might be involved in the regulation of blood pressure. These findings suggest that WTC-*dfk* rats could represent a powerful tool for studying the physiological functions of KCNQ1 and for the establishment of new therapeutic procedures for *Kcnq1*-related diseases.

voltage-dependent potassium channel; deafness; long-QT syndrome; achlorhydria; hypertension

KCNQ1 ENCODES A PORE-FORMING (α) subunit of the voltage-gated K^+ channel. It encodes six membrane-spanning domains (S1–S6), including the voltage sensor (S4) domain, and a K^+-selective pore between S5 and S6 (2, 24). To form native channels, KCNQ1 coassembles with small β-subunits, so-called KCNE proteins. Although the stoichiometry of coassembly is not yet known, it is likely that four α-subunits assemble with four β-subunits to form the channels.

In the heart, KCNQ1 is coassembled with KCNE1. The KCNQ1/KCNE1 complex produces a slowly activating delayed rectifier K^+ current (I_{Ks}) that contributes to the later phase of action potential repolarization, returning to the resting potential (2, 24). Mutations of the human *KCNQ1* gene are associated with the congenital long-QT syndrome, an inherited disorder that is characterized by abnormal ventricular repolarization and increases the risk of sudden death from cardiac arrhythmias. There are at least two familial forms of long-QT syndrome. One is the Jervell and Lange-Nielsen syndrome, which is believed to be inherited as an autosomal recessive trait and associated with congenital deafness (12). A second, more common familial form is inherited as an autosomal dominant trait with no other phenotypic abnormalities. This form, which is sometimes referred to as the Romano-Ward syndrome (34), is usually associated with a lower arrhythmia risk than the autosomal recessive form.

In the inner ear, both KCNQ1 and KCNE1 are expressed. In this tissue, the KCNQ1/KCNE1 complex produces a K^+-rich fluid known as endolymph that bathes the organ of Corti, the cochlear organ responsible for hearing, and the utricle, saccule, and semicircular canal, which are responsible for balance and equilibrium. Functional loss of KCNQ1 provokes congenital deafness in the individuals with Jervell and Lange-Nielsen syndrome. The mechanism of deafness is that the lack of I_{Ks} leads to inadequate endolymph production and deterioration of the organ of Corti (31).

In the stomach, KCNQ1 and KCNE2 are both expressed in the luminal membrane of the acid-secreting parietal cells (6, 11), where H^+/K^+-ATPase, a pump responsible for the transfer of H^+ ions into the stomach, is coexpressed (9). The KCNQ1/KCNE2 complex yields K^+ currents that are activated by acidic pH stimulation at resting membrane potential. Thus KCNQ1/KCNE2 forms acid-activated luminal K^+ channels whose function is to supply K^+ to the luminal surface to allow H^+-for-K^+ exchange by the pump (11). Disruption of *Kcnq1* in mice causes a large increase in stomach pH that is accompanied by gastric hyperplasia (16).

Article published online before print. See web site for date of publication (http://physiolgenomics.physiology.org).

Address for reprint requests and other correspondence: T. Serikawa, Institute of Laboratory Animals, Graduate School of Medicine, Kyoto Univ., Sakyo-ku, Kyoto 606-8501, Japan (e-mail: serikawa@anim.med.kyoto-u.ac.jp).

In the small intestine and colon, KCNQ1 colocalizes with KCNE3 in the basolateral membranes of crypt cells (6). The KCNQ1/KCNE3 complex is constitutively opened at the more negative membrane potential of intestinal epithelial cells and can be further activated by the action of cAMP (25). This complex is thought to be important for maintenance of transepithelial transport in the colon and the small intestine, by recycling K^+ that is transported into the cell by basolateral Na^+-K^+-$2Cl^-$ (NaK2Cl) cotransporters and Na^+/K^+-ATPases. Thus the KCNQ1/KCNE3 channel is required for transepithelial cAMP-stimulated Cl^- secretion.

In the airway epithelia, KCNQ1 mediates a basolateral K^+ conductance that plays an important role in maintaining cAMP-dependent Cl^- secretion (10, 17). The β-subunit coassembled with KCNQ1 in the airway epithelia has been a matter of debate. In the mouse, KCNE3 is thought to be coupled with KCNQ1 (10). In the pancreas, KCNQ1 is expressed in the insulin-secreting cells. Inhibitors for the KCNQ1 channels increase the insulin secretion, which suggested that KCNQ1 would be involved in insulin secretion by the regulation of membrane potentials in the insulin-secreting cells (29).

Kcnq1 expression is not only confined to the tissues described above but also occurs in many epithelial tissues, such as placenta, kidney, liver, and thymus (7, 33, 38). However, no clear functional role of *Kcnq1* in these tissues has been found as yet. For a further understanding of *Kcnq1* functions in these tissues as well as the establishment of novel therapeutic procedures for diseases associated with *Kcnq1* dysfunction, such as the long-QT syndrome, deafness, and achlorhydria, an animal model that is easy to investigate and manipulate is required. To address this issue, a rat model would be suitable, since the rat has an ~10 times larger size than the mouse and offers several unique advantages in various fields of research. In particular, the rat has been used as a variety of disease models because of its easier clinical examination and sampling as well as therapeutic administration and manipulation.

In this report, we describe the characteristics of a novel *Kcnq1* mutation, deafness Kyoto (*dfk*), in the rat. Positional candidate cloning revealed that the *dfk* allele is an intragenic deletion including exon 7 of the *Kcnq1* gene. WTC-*dfk* rats suffer from deafness and imbalance resulting from profound morphological abnormalities of the inner ear. These rats exhibit prolonged QT intervals and T-wave abnormalities on electrocardiogram (ECG) measurements and elevation of pH to almost neutral in the gastric secretion. Additionally, WTC-*dfk* rats display hypertension.

MATERIALS AND METHODS

Animals. Rats showing abnormal behaviors characterized by head tossing, drawing back, stepping back, and circling were found in the $N_{12}F_{10}$ generation of a WTC.ZI-*Atrn*^{z} congenic strain (15) at the Institute of Laboratory Animals, Graduate School of Medicine, Kyoto University, in 1999. Even after elimination of the *Atrn*^{z} mutation on chromosome (Chr) 3 (14), these phenotypes were observed and were inherited in an autosomal recessive manner. These mutant phenotypes resembled behavioral features of some types of deafness mutants. Therefore, we called the causative gene "deafness Kyoto" (gene symbol, "*dfk*"). Because the backcross generation in which the *dfk* mutation was found was sufficient to replace the genetic background with WTC, *dfk* was thought to be synonymous with a mutation arising on the genetic background of an inbred WTC strain. Therefore, WTC-*dfk* and WTC are coisogenic; their genetic backgrounds were identical except for the *dfk* mutation. ACI/NKyo and WTC rat strains were maintained at the Institute of Laboratory Animals, Graduate School of Medicine, Kyoto University. Animal care was conducted according to the Guideline for Animal Experiments of Kyoto University. All experimental procedures were approved by the Animal Research Committee, Graduate School of Medicine, Kyoto University.

The ACI/NKyo (NBRP no. 0001), WTC (NBRP no. 0020), and WTC-*dfk* (NBRP no. 0289) strains have been deposited in the National BioResource Project for the Rat in Japan and can be obtained from the Project (**http://www.anim.med.kyoto-u.ac.jp/nbr/**).

Auditory brainstem response measurement. Auditory brainstem response (ABR) measurements were performed in three individuals each for WTC and WTC-*dfk* rats at 26 wk of age. The following experiments were done on animals that were anesthetized with ketamine hydrochloride (60 mg/kg, im) and pentobarbital sodium (21 mg/kg, ip) and kept at 38 C. Stainless steel needle electrodes were inserted subcutaneously into the vertex (indifferent) and one side (active) and the other side (ground) of the retroauricular region, respectively. The ABR was obtained by averaging 1,000 evoked responses to click stimuli at intensities of 60, 65, 70, 75, 80, 100, 120, and 135 dB peak equivalent sound pressure level (peSPL), with 50-ms intervals generated by an acoustic stimulator (MEB-5504; Nihon Koden, Tokyo, Japan). Clicks were delivered through an inner ear-type earphone facing the meatus acusticus externus.

Genetic mapping. (WTC-*dfk* × ACI)F_1 rats were intercrossed to obtain F_2 rats. Homozygous WTC-*dfk* animals were identified on the basis of appearance of head-tossing and/or circling behaviors and inability to swim at 3–4 wk of age. Two hundred and forty WTC-*dfk* animals were obtained from 1,000 F_2 progeny and used for genetic mapping. For the initial mapping of *dfk*, we employed pooled simple sequence-length polymorphism (SSLP) analysis (27). DNAs from 45 randomly selected rats were standardized to 20 ng/μl, and equal amounts of individual DNAs were pooled. The *dfk* DNA pool was genotyped for 75 microsatellite markers distributed among all autosomes. For the fine mapping of *dfk*, all *dfk/dfk* animals were genotyped.

Sequencing. PCR products were treated with ExoSAP-IT (Amersham Biosciences, Piscataway, NJ) to digest single-strand DNAs and excess primers. Cycle sequencing was performed with the BigDye Terminator Ready Reaction Mix according to the manufacturer's instructions (Applied Biosystems, Fater City, CA). PCR samples were purified with CENTRI-SEP spin columns and were then loaded into an ABI PRISM 3100 genetic analyzer (Applied Biosystems).

Northern blotting. Poly(A) RNA was purified from total RNA by using Oligotex-dT30 Super (Roche Diagnostics). Two micrograms of poly-A RNA were electrophoresed on formaldehyde-denaturing agarose gels and blotted onto Hybond N+ membrane (Amersham Biosciences). Bands on the autoradiograph were detected by using an imaging plate and a computerized image display system (BAS2000; Fuji Film, Tokyo, Japan). A DNA fragment containing exons 9–14 of rat *Kcnq1* was used as a probe.

Electrocardiograms. ECG recordings were obtained from adult (12–18 wk) wild-type (n = 6) and WTC-*dfk* (n = 6) rats using implantable Physiotel TA10EA-F20 radio frequency transmitters and receivers (Data Sciences International, Arden Hills, MN). After an animal was anesthetized with chloral hydrate (600 mg/kg, ip), the transmitter was placed within the peritoneal cavity. The electrodes were placed at the right axilla and at the left side of the xiphoid. Each electrode was sutured subcutaneously. After implantation of the transmitters, the animals were allowed to recover for at least 72 h. Twenty consecutive beats were recorded from individual animals under resting conditions. Unfiltered data were analyzed offline, and QRS, QT, PQ, and RR intervals were measured. Rate-corrected QT values (QTc) were derived using the formula QTc = QT/SQRT(RR/100) (19).

Histopathological analyses. To evaluate the histological phenotype of *dfk* rats, WTC-*dfk* rats were killed under anesthesia at 34 wk of age (n = 3). Age-matched WTC rats (n = 3) were examined as controls.

Perfusion fixation through the left ventricle was performed with 4% paraformaldehyde in 0.1 M phosphate buffer. Brains, spinal cords, inner ears, stomach, and representative visceral organs were removed and fixed with the same fixative solution. Before processing for paraffin embedding, the ear tissues were decalcified with 5% EDTA-dipotassium salt. The samples were embedded in paraffin, and sections (4 μm) were stained with hematoxylin and eosin stain (HE). The cochlea was also embedded in epoxy resin, and then semithin sections (1 μm) were stained with toluidine blue.

Stomach pH and acid output measurements. The WTC-*dfk* rats (11 wk old, $n = 5$) and the age-matched, wild-type, control WTC rats ($n = 5$) were fasted overnight before the experiment with free access to water. Each rat was anesthetized, and the abdominal cavity was opened and the pylorus ligated. Four hours after treatment, the rat was killed and the stomach was removed. The intraluminal contents were drained into a centrifuge tube after a small nick was made in the stomach wall along the greater curvature adjacent to the pyloric ligature. The solutions with the stomach contents were centrifuged to pellet the insoluble material. The pH of the supernatants was measured, and then acid was titrated using an automatic titrator COMTITE-500 (Hiranuma Sangyo, Ibaraki, Japan). The results were expressed as microequivalents of acid per liter of gastric volume.

Blood pressure measurement. Systolic blood pressure was measured by the tail-cuff method using a nonpreheated, noninvasive blood pressure monometer (MK-2000; Muromachi Kikai, Tokyo, Japan). The average values of three measurements were determined for individual animals. All measurements were performed on 11 male rats at 9 or 10 wk of age (18).

RESULTS

Clinical features of WTC-dfk rats. The *dfk* rats were recognized at 10 days after birth by their twisting of their necks toward the back when lifted by the tail. After weaning, they exhibited hyperactivity and usually showed rapid head bobbing and occasionally a head tilt. Mature WTC-*dfk* rats displayed bidirectional circling behavior. In addition, they were unable to swim. When WTC-*dfk* rats were placed into a deep tank filled with warm water, WTC-*dfk* rats immediately began rotating along their long axis and sank underwater. While underwater, the rats were still rotating along their body length. The rats seldom resurfaced until they were rescued. These findings suggested that WTC-*dfk* rats might have lost their balance and have defects in the inner ear, which is responsible for linear and angular acceleration.

The adult WTC-*dfk* rats seemed to be smaller than the normal littermates, so we measured the body weights of the WTC-*dfk* rats (male, $n = 6$) at 5, 6, and 10 wk of age. At 5 or 6 wk of age, body weights were not significantly different between WTC and WTC-*dfk* rats. At 10 wk of age, WTC-*dfk* rats showed significantly lower body weight than WTC rats (246.3 ± 3.2 vs. 190.6 ± 8.8 g, $P < 0.01$) (Fig. 1*A*).

ABR. In addition to the imbalance, WTC-*dfk* rats showed no response to sounds such as rapping and clapping. To test the

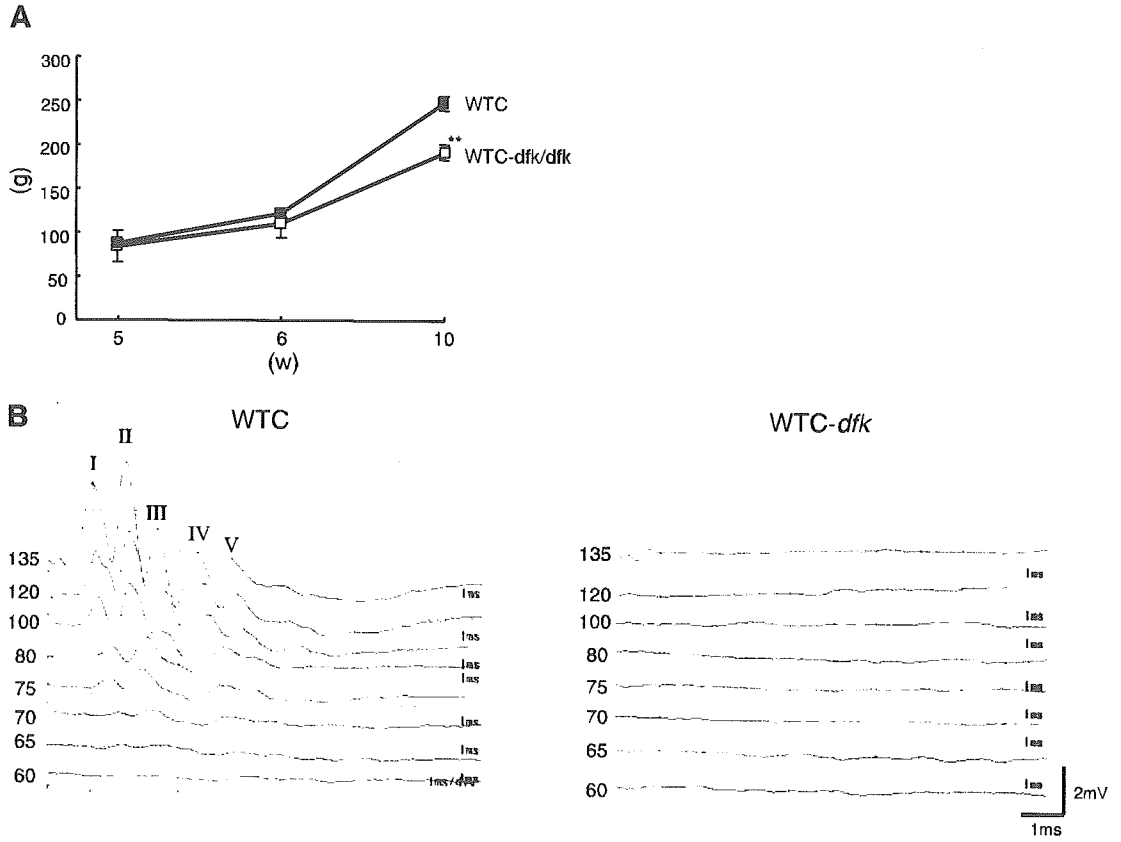

Fig. 1. Body weight and auditory phenotypes of the WTC-*dfk* rat. *A*: body weights of WTC and WTC-*dfk* rats. Body weights were measured in male WTC ($n = 6$) and male WTC-*dfk* ($n = 6$) rats at 5, 6, and 10 wk (w) of age. Impaired gain of body weight was observed in WTC-*dfk* rats at 10 wk of age. *B*: representative auditory brainstem response (ABR) of the WTC and WTC-*dfk* rats. The 5 major peaks (labeled *I*, *II*, *III*, *IV*, and *V*) were clearly detectable with >100 dB in the WTC rat (*left*), whereas no waveform was recorded at the highest stimulus level of 135 dB in the WTC-*dfk* rat (*right*). ABR measurements were performed in WTC ($n = 3$) and WTC-*dfk* ($n = 3$) rats at 26 wk of age.

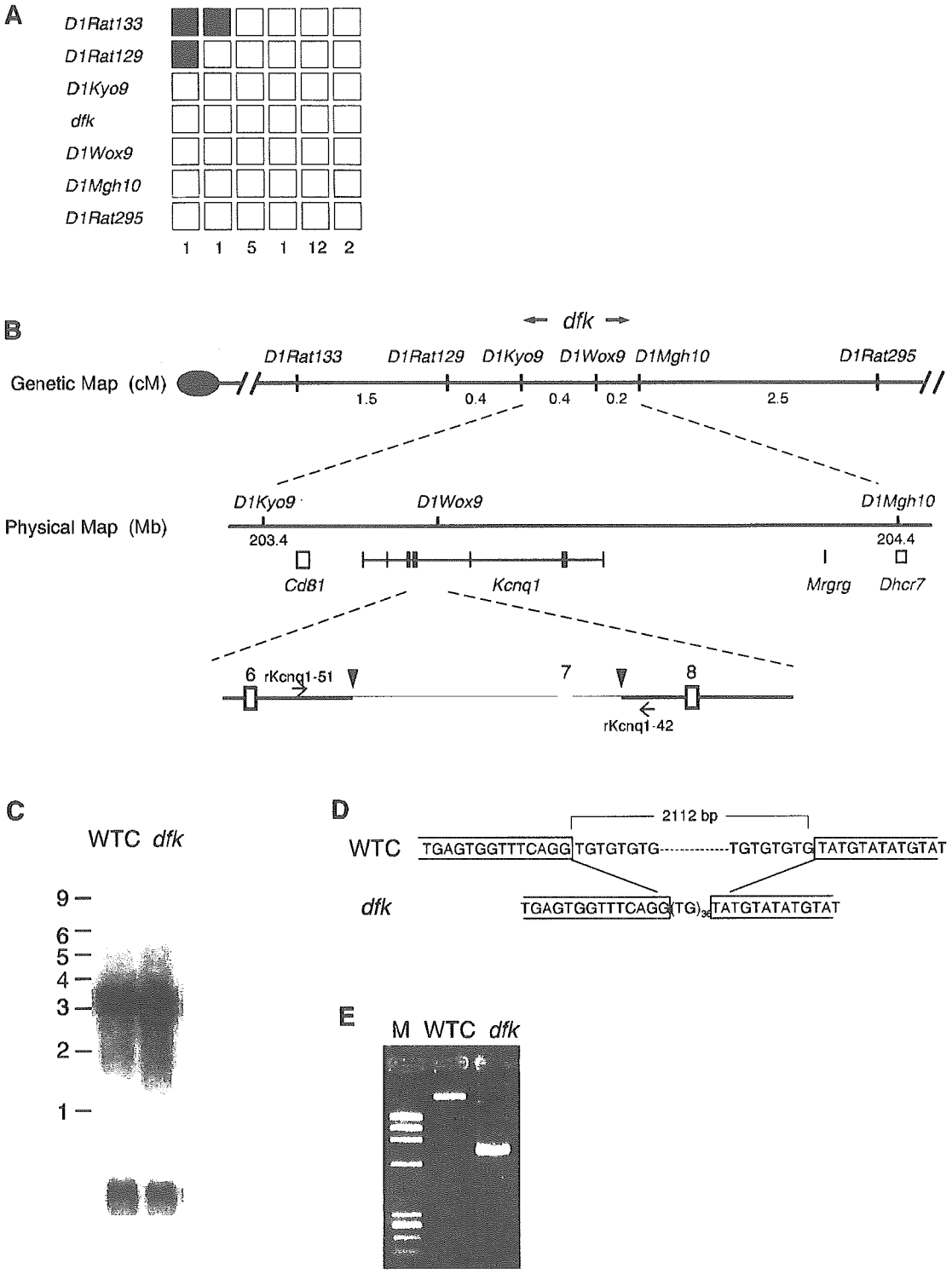

Fig. 2. Positional cloning of the *dfk* mutation. *A*: distribution of haplotypes observed among 22 *dfk*-homozygous F_2 progeny carrying a recombinant chromosome between *D1Rat133* and *D1Rat295*. White boxes, homozygote for the WTC allele. Grey boxes, heterozygote. Black boxes, homozygote for the ACI allele. *B*: *dfk* was genetically mapped to 0.8-cM region between *D1Kyo9* and *D1Mgh10*. The *dfk* showed no recombination with *D1Wox9* in 480 informative meioses. The *dfk* locus was physically localized to the ~1-Mb region defined with *D1Kyo9* and *D1Mgh10*. Within the *dfk* locus, 4 genes have been mapped. In the WTC-*dfk* rats, a genomic sequence containing *Kcnq1* exon 7 was deleted. The 5′- and 3′-breakpoints of the deleted sequence are indicated by arrowheads. *C*: expression of *Kcnq1* assessed by Northern blot analysis. Poly(A) RNAs from the hearts of WTC and WTC-*dfk* rats are hybridized with a probe containing exons 9–14 of rat *Kcnq1*. A smaller *Kcnq1* transcript due to the loss of exon 7 was observed in WTC-*dfk*. Hybridization signals of β-actin on the same blot are shown at *bottom*. Molecular weight markers are indicated to the *left* in kilobases. *D*: genomic sequences around the breakpoints of the *dfk* deletion. A 2,040-bp sequence containing the *Kcnq1* exon 7 was deleted in the WTC-*dfk* genome. *E*: molecular diagnosis of the *dfk* deletion. With use of the primers rKcnq1–51 and rKcnq1–42, a 2,735-bp PCR product was obtained from the WTC genome, while a 695-bp fragment was obtained from the WTC-*dfk* genome.

auditory organ function, we measured ABR in WTC-*dfk* and WTC rats. In WTC rats, ABR composed of I, II, III, IV, and V peaks was observed with intensity of over 100 dB (Fig. 1*B*). The WTC rats showed an average hearing threshold of 68.3 ± 2.58 dB, whereas all WTC-*dfk* rats exhibited no ABR up to the maximum level (>135 dB) of acoustic stimulation (Fig. 1*B*), indicating that WTC-*dfk* rats were completely deaf.

Identification of the dfk mutation. The pooled SSLP analysis showed a linkage relationship between *D1Rat429* and the *dfk* locus. A genetic linkage study of 240 WTC-*dfk* rats using 19 additional markers on Chr 1 narrowed down *dfk* to a 0.8-cM interval between *D1Kyo9* and *D1Mgh10* (Fig. 2, *A* and *B*). The *dfk* gene showed no recombination with *D1Wox9* in 480 informative meioses. Within the *dfk* locus, four genes, *Cd81* (CD 81 antigen), *Kcnq1* (potassium voltage-gated channel, subfamily Q, member 1), *Mrgrg* (Mas-related G-protein coupled receptor member G), and *Dhcr7* (7-dehydrocholesterol reductase), have been mapped, and these genes were thought to be candidates for *dfk*.

Because human *KCNQ1* mutation is associated with deafness (22), and *Kcnq1*-deficient mice showed similar behavioral phenotypes to those of WTC-*dfk* rats (5), *Kcnq1* was considered to be the strongest candidate. Northern blot analyses showed that *Kcnq1* transcript of the WTC-dfk was smaller than that of WTC (Fig. 2*C*). Sequencing analyses of the entire coding region and all of the exon-intron boundaries of *Kcnq1* revealed that the entire exon 7 and its flanking sequences were lacking in the WTC-*dfk* rats. The deletion was 2,040 bp in length and flanked with TG dinucleotide tandem repeats (Fig. 2*D*). No nucleotide alternations were observed in the coding sequences of either the *Cd81*, *Mrgrg*, or *Dhcr7* genes between WTC and WTC-*dfk* rats.

To verify and diagnose the deletion at the molecular level, we designed the PCR primers rKcnq1–51 (5′-ACCTGTCATGGCTCCCTAGA-3′) and rKcnq1–42 (5′-AGGCTGTCCTCAGCAAGAAG-3′), which are located outside of the 5′- and 3′-breakpoints, respectively (Fig. 2*B*). These primers yielded a 695-bp PCR product from WTC-*dfk* and a 2,735-bp PCR product from the wild-type WTC (Fig. 2*E*).

Histopathology of the inner ear. To identify the histopathological alterations responsible for the deafness and imbalance observed in WTC-*dfk* rats, we examined the inner ear struc-

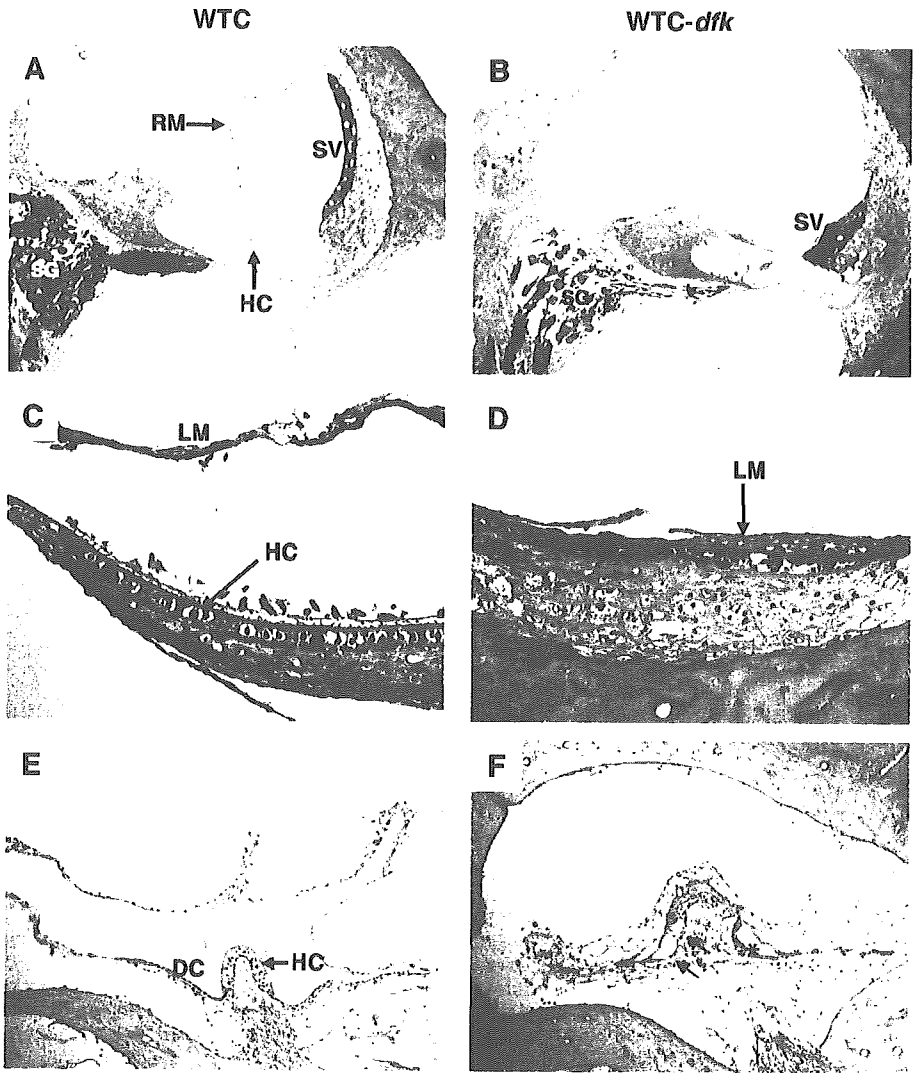

Fig. 3. Histological features of the inner ear of WTC and WTC-*dfk* rats. *A* and *B*: epon-embedded sections of the cochlea stained with toluidine blue. Note that collapsed Reissner's membrane, atrophied stria vascularis, loss of hair cells, and marked reduction of neurons in the spiral ganglion are observed in the 34-wk-old WTC-*dfk* rat. *C* and *D*: details of the saccule macula. Note that the membranous labyrinth is collapsed onto the macula and compresses the statoconia, statoconial membrane, and hair cells in the 34-wk-old WTC-*dfk* rat. *E* and *F*: details of the ampullary crest. Note that the membranous labyrinth is collapsed onto the cupula. A small cavity is present between the membrane and the cupula (indicated by an asterisk), and vacuoles are seen in the marginal region of the ampullary crest (indicated by arrows) in the 34-wk-old WTC-*dfk* rats. DC, dark cell; HC, hair cell; LM, membranous labyrinth; RM, Reissner's membrane; SG, spiral ganglion; SV, stria vascularis.

Table 1. *Comparison of ECG parameters in WTC and WTC-dfk rats*

Parameter	WTC	WTC-*dfk*
HR, bpm	319.4±30.9	350.4±31.1
RR, ms	189.0±16.9	174.2±17.7
PQ, ms	42.3±2.8	40.8±3.6
QRS, ms	15.8±1.9	15.9±2.5
QT, ms	63.7±13.7	86.8±13.7*
QTc, ms	46.4±10.1	65.8±9.2†

All data are presented as means ± SD. Data sets were obtained from adult (12–18 wk) WTC (n = 6) and WTC-*dfk* (n = 6) rats and were compiled using Student's t-test. HR, heart rate; bpm, beats/min; QTc, rate-corrected QT values. *$P < 0.05$ vs. WTC. †$P < 0.01$ vs. WTC.

Table 2. *Acidity of stomach contents in WTC and WTC-dfk rats*

Parameter	WTC	WTC-*dfk*
Gastric volume, ml	2.8±0.9	2.5±0.7
pH	1.47±0.1	7.24±0.2†
Acidity, meq/l	84.2±18.6	ND

All data are presented as means ± SD. Data sets were obtained from WTC (n = 5) and WTC-*dfk* (n = 5) rats at 11 wk of age and were compiled using Student's t-test. ND, not detected. †$P < 0.01$ vs. WTC.

tures. In the cochlea of the 34-wk-old WTC-*dfk* rats, the Reissner's membrane was collapsed and the volume of the cochlear duct was markedly reduced. The stria vascularis was severely atrophied. The inner and outer hair cells in the Corti were degenerated, and swelling of supporting cells was observed. The number of neurons in the spiral ganglion was markedly reduced (Fig. 3*B*). In the macula statica of the utricle, the membranous labyrinth was collapsed onto the macula. The statoconia, the statoconial membrane, and the hair cells were compressed by the collapsed membranous labyrinth, and the endolymphatic space was not observed. The hair cells and supporting cells were severely disarrayed (Fig. 3*D*). In the ampullary crest of the semicircular ducts, the membranous labyrinth was also collapsed and the endolymphatic space was dramatically reduced. The collapsed membranous labyrinth compressed the sensory hair cells and the KCNQ1-expressing dark cells. Vacuoles were observed in the hair cells located in the marginal region of the ampullary crest (Fig. 3*F*).

Prolonged QTc interval in WTC-dfk rats. To evaluate *Kcnq1* function in the rat heart, we examined the ECGs in WTC and WTC-*dfk* rats. Twenty consecutive beats were measured in individual resting animals to obtain the mean values, because ECGs in conscious animals were likely to be contaminated by muscle artifact and noise. The QT interval was measured from the beginning of the QRS complex to the end of T wave, defined as the point where the T wave merges with the isoelectric line, as described previously (5). The WTC-*dfk* rats demonstrated significant increases in QT and QTc intervals, although there were no significant differences in other parameters such as HR, RR, PQ, and QRS (Table 1). The most striking change in WTC-*dfk* rats occurred in the form of the T wave (Fig. 4). The peak of the T wave was prolonged, and the T-wave area was increased compared with that of WTC rats.

Gastric abnormalities in WTC-dfk rats. To evaluate *Kcnq1* function in the rat stomach, we examined gastric functions of the WTC-*dfk* rats. The volume of the secretion products in the pylorus-ligated stomach collected during the 4-h experimental period was not different between WTC-*dfk* and WTC rats. However, the pH of the stomach fluids was elevated to almost neutral (pH = 7.24 ± 0.2) in the WTC-*dfk* rats, whereas the WTC stomach retained strong acidity (pH = 1.47 ± 0.1). The acidity of the stomach contents could not be detected in the WTC-*dfk* rats, while the acidity of the WTC stomach was 84.2 ± 18.6 meq/l (Table 2). These findings indicated that acid production was impaired in the WTC-*dfk* rats.

The most prominent pathological feature in the stomach of 34-wk-old WTC-*dfk* rats was the appearance of hypertrophic gastric glands in the mucosa of the stomach body (Fig. 5, *B* and *C*). Such lesions were scattered in the mucosa, and their cytoplasm was deeply stained with eosin. Additionally, dilatation of the fundic glands and fibrosis in the lamina propria were observed in the stomach body of WTC-*dfk* rats. Fibrosis was

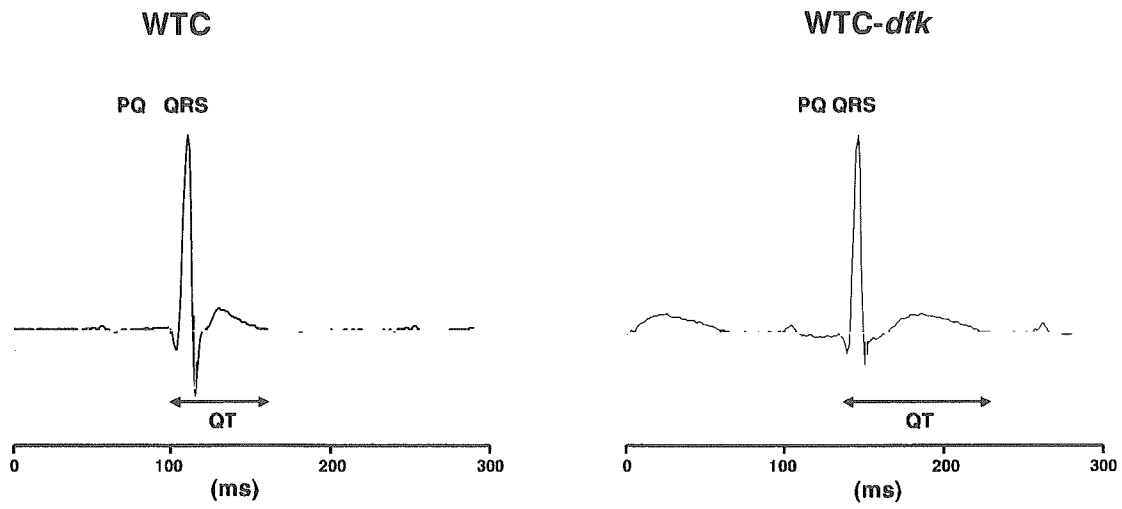

Fig. 4. Representative surface electrocardiogram (ECG) trace recorded in vivo in WTC and WTC-*dfk* rats. Representative ECG traces obtained from adult (12–18 wk) WTC (n = 6) and WTC-dfk (n = 6) rats. Each parameter (PQ, QRS, QT) is indicated. Note that the QT interval was prolonged in WTC-*dfk* compared with the wild-type coisogenic control WTC rat. Depicted tracings were selected as representative of the particular phenotype.

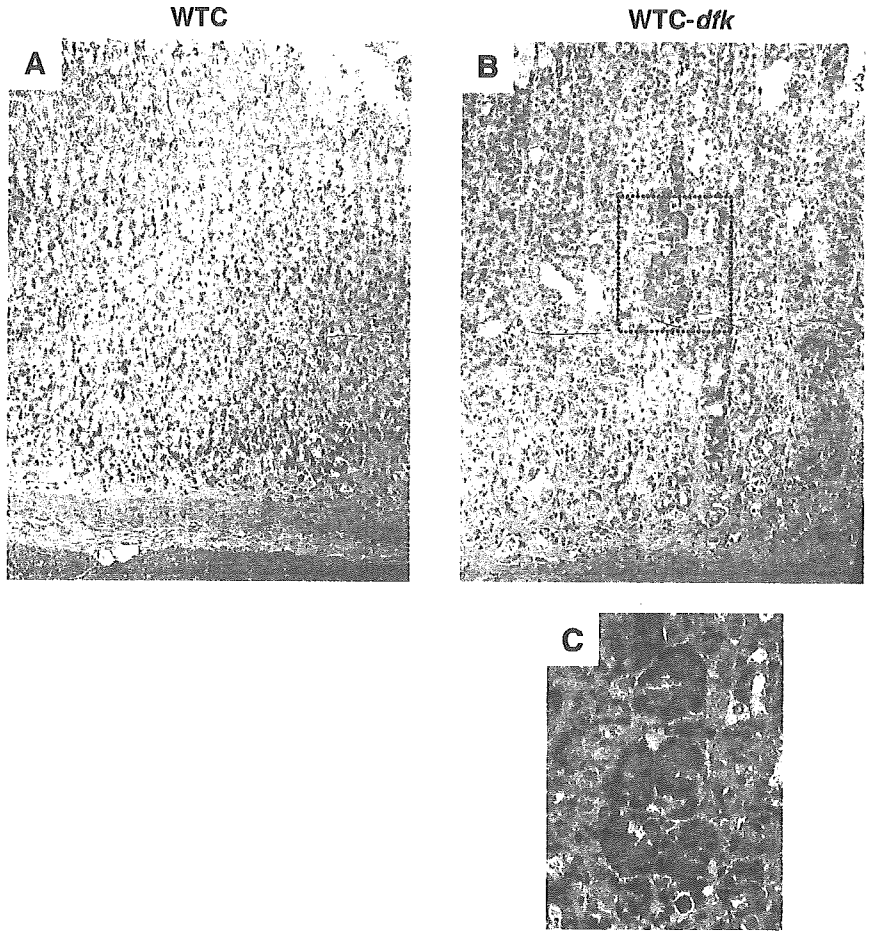

Fig. 5. Histopathological features of the stomach of WTC and WTC-*dfk* rats. Mucosa of the stomach body of a 34-wk-old WTC rat (*A*) and WTC-*dfk* rat (*B*). Note that hypertrophic eosinophilic cells, scattered in the mucosa, are found in the WTC-*dfk* rat. Fibrosis was distributed in the lamina propria, especially in the bottom part of the mucosa. *C*: Higher magnification of the hypertrophic eosinophilic cells.

prominent at the bottom part of the mucosa (Fig. 5*B*). No pathological alteration was observed in the pylorus of the WTC-*dfk* rats.

Hypertension in WTC-dfk rats. To examine the physiological phenotypic characteristics of the WTC-*dfk* rats, we collected phenotypic data about blood pressure, biochemical blood test values, hematology, and urology. The most striking finding was hypertension in the WTC-*dfk* rats. They showed significant increases in the systolic blood pressure (SBP) compared with WTC (165.8 ± 22 vs. 125.8 ± 14.4 mmHg, $P = 0.0001$). The blood pressure level of WTC-*dfk* rats was highly placed on the ranking list of the SBP of 98 rat inbred strains of the Rat Phenome Project of the NBRP in Japan (**http://www.anim.med.kyoto-u.ac.jp/nbr**) (18). The SBP of WTC-*dfk* rats was greater than the mean value plus one standard deviation of the SBP of the 98 rat strains (142.7 ± 19.4 mmHg), while that of WTC rats was within the mean value plus one standard deviation.

DISCUSSION

We have described here the molecular basis and phenotypes of a novel mutation of the rat *Kcnq1* gene. WTC-*dfk* rats had an intragenic deletion that included whole exon 7 of the *Kcnq1* gene. The rat *Kcnq1* cDNA encodes a 669-amino acid polypeptide with six membrane-spanning segments and a pore-associated domain (13). *Kcnq1* exon 7 is 111 bp in length and encodes a 37-amino acid peptide that forms a pore-associated domain and part of the sixth transmembrane domain. Therefore, the *dfk* deletion allele was thought to result in a smaller protein that lacked the pore, which plays important roles in generating K^+ current.

We found several intriguing phenotypes of the WTC-*dfk* rat. First, these rats showed circular movements, imbalance, and complete deafness. Histological analyses demonstrated the marked reduction of the endolymph of the inner ear and the collapse of sensory hair cells. These findings implied that endolymph reduction followed by hair cell collapses resulted in inner ear defects in the WTC-*dfk* rats. *Kcnq1*-deficient mice also show circular movements, imbalance, deafness, and inner ear pathologies that are very similar to those observed in the WTC-*dfk* rats (5, 16). The phenotypic similarities and deduced functions of the mutated KCNQ1 of the WTC-*dfk* rat suggested that WTC-*dfk* rats would be deficient for KCNQ1 protein.

Second, the WTC-*dfk* rats manifested prolonged QT interval and abnormal T-wave form in the ECG, indicating that the ventricular repolarization was prolonged in the WTC-*dfk* rats. The ventricular repolarization derives from transient outward K^+ currents (I_{to}) and delayed, outwardly rectifying K^+ currents (I_K) (21). In the rat myocytes, two transient outward K^+ currents, $I_{to,f}$ and $I_{to,s}$ (1, 36), and five distinct delayed rectifier currents, I_{Kr}, I_{Kur}, I_K, $I_{K,slow}$, and I_{ss}, have been identified (1, 3, 20). However, I_{Ks} current generated from KCNQ1/KCNE1

complex is not a prominent repolarizing current in adult rats or in mice. Therefore, the cardiac phenotype seen in the WTC-*dfk* rats would not be a direct effect of KCNQ1 deficiency but would be induced by extracardiac stimuli such as autonomic nerve and hormonal factors (32, 35). This idea is supported by the data on the cardiac phenotypes of the *Kcnq1*-deficient mice. They displayed abnormal T-wave form and prolongation of the QT interval when measured in vivo, but not in isolated hearts (5). In addition, nicotine challenge of the isolated heart and acute stress due to saline injection in vivo revealed that sympathetic stimulation induced a long-QT phenotype in *Kcnq1*-deficient mice (28).

Third, we found achlorhydria in the WTC-*dfk* rats. Because gastric H^+ is secreted by the H^+/K^+-ATPase with coupling to the uptake of the luminal K^+ (23, 37), it is possible that the mutated KCNQ1 polypeptide fails to transport K^+ into the gastric lumen. Histological findings of the WTC-*dfk* stomach were hypertrophy of the gastric glands and fibrosis in the lamina propria. Because the administration of proton pump inhibitor sometimes induces hypertrophic gastric glands in the rat, these pathological changes are thought to have been produced as a direct effect of the elevation of pH in the stomach (4). *Kcnq1*-deficient mice also show achlorhydria and increased weight of the stomach resulting from mucous neck cell hyperplasia (8, 16).

It is likely that the lower body weight found in the WTC-*dfk* rats is related to their hyperactivity associated with the inner ear defects. Additionally, the loss of *Kcnq1* functions in the stomach, the intestine, or the pancreas might give another possible explanation. Gastric H^+ is required to converse pepsinogen to pepsin, the protease largely responsible for initiating the digestion of proteins in the stomach. KCNQ1 expressed in the epithelium of the small intestine and colon is believed to regulate K^+ transport into the lumen (25). Luminal K^+ is required for transepithelial Cl^- secretion, which regulates the osmolality of the intestinal or colonic mucus. In the insulin-secreting cells, the KCNQ1 channels might play a role in regulation of the insulin secretion (29). Thus investigating the digestive capability and insulin secretion levels in the WTC-*dfk* rats would be helpful for determining the cause of the lower body weight.

Lastly, the WTC-*dfk* rats displayed hypertension. This is the first evidence that *Kcnq1* might be involved in the regulation of blood pressure in the rat. Hypertension is provoked by a variety of etiologies. We have not yet determined which factor(s) induces hypertension in the WTC-*dfk* rats, but it seems likely that it is due to a defect in reabsorption in the proximal tubule of the kidney. In the mouse kidney, KCNQ1 colocalizes with KCNE1 in the brush border of the mid to late proximal convoluted tubule as well as in the proximal straight tubule (30). It is thought that the KCNQ1/KCNE1 complex would make K^+ flux to the lumen, which is essential to counteract membrane depolarization due to electrogenic Na^+-coupled transport (30). Considering the important role of reabsorption in the regulation of blood pressure, it is possible that there might be some defect(s) in the kidney proximal tubule of the WTC-*dfk* rats.

WTC-*dfk* rats offer a sophisticated genetic system for studies of the physiological functions of KCNQ1, because this strain has a strict control strain, WTC. The two strains are coisogenic and have an identical genetic background except for the *dfk* deletion. Thus phenotypic differences found between them would only result from the *dfk* mutation, which would imply the involvement of the *Kcnq1* in such phenotypes. This genetic system was obtained simply by a spontaneous mutation arising in an inbred strain. In the gene knockout mouse, one cannot exclude effects of genes closely linked to the targeted gene on their phenotypes, even after producing congenic strains (26). *Kcnq1* has been shown to be associated with several diseases such as long QT, deafness, achlorhydria, and hypertension. To develop more effective treatments for these disorders, WTC-*dfk* could offer a powerful new tool as a *Kcnq1*-related disease model. Furthermore, because KCNQ1 is expressed in various epithelial tissues, including lung, colon, small intestine, and thymus (7, 33), the functions of KCNQ1 in these tissues could be clarified using the coisogenic system of WTC-*dfk* and WTC.

ACKNOWLEDGMENTS

We are thankful to the National BioResource Project for the Rat in Japan (**http://www.anim.med.kyoto-u.ac.jp/nbr/**) for providing rat strains (ACI/NKyo, WTC, and WTC-*dfk*).

Present address of K. Kitada: Laboratory of Mammalian Genetics, Center for Advanced Science and Technology, Hokkaido University, Kita 10 Nishi 8, Kita-ku, 060-0810 Sapporo, Japan.

GRANTS

This work was supported in part by Grants-in-Aid for Scientific Research from the Japan Society for the Promotion of Science (no. 15300141 to T. Kuramoto and no. 16200029 to T. Serikawa) and by a Grant-in-Aid for Cancer Research from the Ministry of Health, Labour and Welfare of Japan.

REFERENCES

1. **Apkon M and Nerbonne JM.** Characterization of two distinct depolarization-activated K^+ currents in isolated adult rat ventricular myocytes. *J Gen Physiol* 97: 973–1011, 1991.
2. **Barhanin J, Lesage F, Guillemare E, Fink M, Lazdunski M, and Romey G.** K(V)LQT1 and IsK (minK) proteins associate to form the *I*(Ks) cardiac potassium current. *Nature* 384: 78–80, 1996.
3. **Boyle WA and Nerbonne JM.** Two functionally distinct 4-aminopyridine-sensitive outward K^+ currents in rat atrial myocytes. *J Gen Physiol* 100: 1041–1067, 1992.
4. **Carlsson E, Larsson H, Mattsson H, Ryberg B, and Sundell G.** Pharmacology and toxicology of omeprazole—with special reference to the effects on the gastric mucosa. *Scand J Gastroenterol Suppl* 118: 31–38, 1986.
5. **Casimiro MC, Knollmann BC, Ebert SN, Vary JC Jr, Greene AE, Franz MR, Grinberg A, Huang SP, and Pfeifer K.** Targeted disruption of the *Kcnq1* gene produces a mouse model of Jervell and Lange-Nielsen Syndrome. *Proc Natl Acad Sci USA* 98: 2526–2531, 2001.
6. **Dedek K and Waldegger S.** Colocalization of KCNQ1/KCNE channel subunits in the mouse gastrointestinal tract. *Pflügers Arch* 442: 896–902, 2001.
7. **Demolombe S, Franco D, de Boer P, Kuperschmidt S, Roden D, Pereon Y, Jarry A, Moorman AF, and Escande D.** Differential expression of KvLQT1 and its regulator IsK in mouse epithelia. *Am J Physiol Cell Physiol* 280: C359–C372, 2001.
8. **Else CM, Lu X, Culiat CT, Rutledge JC, Cacheiro NL, Generoso WM, and Stubbs LJ.** Heightened susceptibility to chronic gastritis, hyperplasia and metaplasia in *Kcnq1* mutant mice. *Hum Mol Genet* 13: 2813–2821, 2004.
9. **Grahammer F, Herling AW, Lang HJ, Schmitt-Graff A, Wittekindt OH, Nitschke R, Bleich M, Barhanin J, and Warth R.** The cardiac K^+ channel KCNQ1 is essential for gastric acid secretion. *Gastroenterology* 120: 1363–1371, 2001.
10. **Grahammer F, Warth R, Barhanin J, Bleich M, and Hug MJ.** The small conductance K^+ channel, KCNQ1: expression, function, and subunit composition in murine trachea. *J Biol Chem* 276: 42268–42275, 2001.
11. **Heitzmann D, Grahammer F, von Hahn T, Schmitt-Graff A, Romeo E, Nitschke R, Gerlach U, Lang HJ, Verrey F, Barhanin J, and Warth**

R. Heteromeric KCNE2/KCNQ1 potassium channels in the luminal membrane of gastric parietal cells. *J Physiol* 561: 547–557, 2004.

12. **Jervell A and Lange-Nielsen F.** Congenital deaf-mutism, functional heart disease with prolongation of the Q-T interval and sudden death. *Am Heart J* 54: 59–68, 1957.
13. **Kunzelmann K, Hubner M, Schreiber R, Levy-Holzman R, Garty H, Bleich M, Warth R, Slavik M, von Hahn T, and Greger R.** Cloning and function of the rat colonic epithelial K^+ channel KVLQT1. *J Membr Biol* 179: 155–164, 2001.
14. **Kuramoto T, Kitada K, Inui T, Sasaki Y, Ito K, Hase T, Kawagachi S, Ogawa Y, Nakao K, Barsh GS, Nagao M, Ushijima T, and Serikawa T.** *Attractin/mahogany/zitter* plays a critical role in myelination of the central nervous system. *Proc Natl Acad Sci USA* 98: 559–564, 2001.
15. **Kuramoto T, Yamasaki K, Kondo A, Nakajima K, Yamada M, and Serikawa T.** Production of WTC/ZI-*zi* rat congenic strain and its pathological and genetic analyses. *Exp Anim* 47: 75–81, 1998.
16. **Lee MP, Ravenel JD, Hu RJ, Lustig LR, Tomaselli G, Berger RD, Brandenburg SA, Litzi TJ, Bunton TE, Limb C, Francis H, Gorelikow M, Gu H, Washington K, Argani P, Goldenring JR, Coffey RJ, and Feinberg AP.** Targeted disruption of the *Kvlqt1* gene causes deafness and gastric hyperplasia in mice. *J Clin Invest* 106: 1447–1455, 2000.
17. **Mall M, Wissner A, Schreiber R, Kuehr J, Seydewitz HH, Brandis M, Greger R, and Kunzelmann K.** Role of K(V)LQT1 in cyclic adenosine monophosphate-mediated Cl^- secretion in human airway epithelia. *Am J Respir Cell Mol Biol* 23: 283–289, 2000.
18. **Mashimo T, Voigt B, Kuramoto T, and Serikawa T.** Rat Phenome Project: the untapped potential of existing rat strains. *J Appl Physiol* 98: 371–379, 2005.
19. **Mitchell GF, Jeron A, and Koren G.** Measurement of heart rate and Q-T interval in the conscious mouse. *Am J Physiol Heart Circ Physiol* 274: H747–H751, 1998.
20. **Nerbonne JM.** Molecular basis of functional voltage-gated K^+ channel diversity in the mammalian myocardium. *J Physiol* 525: 285–298, 2000.
21. **Nerbonne JM and Kass RS.** Physiology and molecular biology of ion channels contributing to ventricular repolarization. In: *Cardiac Repolarization. Bridging Basic and Clinical Science*, edited by Gussal IB and Antzelevitch C. Totowa, NJ: Humana, 2003, p. 25–62.
22. **Neyroud N, Tesson F, Denjoy I, Leibovici M, Donger C, Barhanin J, Faure S, Gary F, Coumel P, Petit C, Schwartz K, and Guicheney P.** A novel mutation in the potassium channel gene KVLQT1 causes the Jervell and Lange-Nielsen cardioauditory syndrome. *Nat Genet* 15: 186–189, 1997.
23. **Reenstra WW and Forte JG.** Characterization of K^+ and Cl^- conductances in apical membrane vesicles from stimulated rabbit oxyntic cells. *Am J Physiol Gastrointest Liver Physiol* 259: G850–G858, 1990.
24. **Sanguinetti MC, Curran ME, Zou A, Shen J, Spector PS, Atkinson DL, and Keating MT.** Coassembly of K(V)LQT1 and minK (IsK) proteins to form cardiac *I*(Ks) potassium channel. *Nature* 384: 80–83, 1996.
25. **Schroeder BC, Waldegger S, Fehr S, Bleich M, Warth R, Greger R, and Jentsch TJ.** A constitutively open potassium channel formed by KCNQ1 and KCNE3. *Nature* 403: 196–199, 2000.
26. **Silver LM.** *Mouse Genetics*. New York: Oxford Univ. Press, 1995.
27. **Taylor BA, Navin A, and Phillips SJ.** PCR-amplification of simple sequence repeat variants from pooled DNA samples for rapidly mapping new mutations of the mouse. *Genomics* 21: 626–632, 1994.
28. **Tosaka T, Casimiro MC, Rong Q, Tella S, Oh M, Katchman AN, Pezzullo JC, Pfeifer K, and Ebert SN.** Nicotine induces a long QT phenotype in *Kcnq1*-deficient mouse hearts. *J Pharmacol Exp Ther* 306: 980–987, 2003.
29. **Ullrich S, Su J, Ranta F, Wittekindt OH, Ris F, Rosler M, Gerlach U, Heitzmann D, Warth R, and Lang F.** Effects of *I*(Ks) channel inhibitors in insulin-secreting INS-1 cells. *Pflügers Arch* 451: 428–436, 2005.
30. **Vallon V, Grahammer F, Richter K, Bleich M, Lang F, Barhanin J, Volkl H, and Warth R.** Role of KCNE1-dependent K^+ fluxes in mouse proximal tubule. *J Am Soc Nephrol* 12: 2003–2011, 2001.
31. **Vetter DE, Mann JR, Wangemann P, Liu J, McLaughlin KJ, Lesage F, Marcus DC, Lazdunski M, Heinemann SF, and Barhanin J.** Inner ear defects induced by null mutation of the isk gene. *Neuron* 17: 1251–1264, 1996.
32. **Walsh KB and Kass RS.** Regulation of a heart potassium channel by protein kinase A and C. *Science* 242: 67–69, 1988.
33. **Wang Q, Curran ME, Splawski I, Burn TC, Millholland JM, VanRaay TJ, Shen J, Timothy KW, Vincent GM, de Jager T, Schwartz PJ, Toubin JA, Moss AJ, Atkinson DL, Landes GM, Connors TD, and Keating MT.** Positional cloning of a novel potassium channel gene: KVLQT1 mutations cause cardiac arrhythmias. *Nat Genet* 12: 17–23, 1996.
34. **Ward OC.** A new familial cardiac syndrome in children. *J Ir Med Assoc* 54: 103–106, 1964.
35. **Washizuka T, Horie M, Watanuki M, and Sasayama S.** Endothelin-1 inhibits the slow component of cardiac delayed rectifier K^+ currents via a pertussis toxin-sensitive mechanism. *Circ Res* 81: 211–218, 1997.
36. **Wickenden AD, Jegla TJ, Kaprielian R, and Backx PH.** Regional contributions of Kv1.4, Kv4.2, and Kv4.3 to transient outward K^+ current in rat ventricle. *Am J Physiol Heart Circ Physiol* 276: H1599–H1607, 1999.
37. **Wolosin JM and Forte JG.** Stimulation of oxyntic cell triggers K^+ and Cl^- conductances in apical H^+-K^+-ATPase membrane. *Am J Physiol Cell Physiol* 246: C537–C545, 1984.
38. **Yang WP, Levesque PC, Little WA, Conder ML, Shalaby FY, and Blanar MA.** KvLQT1, a voltage-gated potassium channel responsible for human cardiac arrhythmias. *Proc Natl Acad Sci USA* 94: 4017–4021, 1997.

Research article

Uterine sensitization-associated gene–1 (USAG-1), a novel BMP antagonist expressed in the kidney, accelerates tubular injury

Motoko Yanagita,[1] Tomohiko Okuda,[1] Shuichiro Endo,[2] Mari Tanaka,[2] Katsu Takahashi,[3] Fumihiro Sugiyama,[4] Satoshi Kunita,[4] Satoru Takahashi,[4] Atsushi Fukatsu,[5] Masashi Yanagisawa,[6,7] Toru Kita,[2] and Takeshi Sakurai[6,8]

[1]COE Formation for Genomic Analysis of Disease Model Animals with Multiple Genetic Alterations, [2]Department of Cardiovascular Medicine, and [3]Department of Oral and Maxillofacial Surgery, Graduate School of Medicine, Kyoto University, Kyoto, Japan. [4]Laboratory Animal Resource Center, Institute of Basic Medical Sciences, University of Tsukuba, Ibaraki, Japan. [5]Department of Artificial Kidneys, Graduate School of Medicine, Kyoto University, Kyoto, Japan. [6]Yanagisawa Orphan Receptor Project, Exploratory Research for Advanced Technology (ERATO), Japan Science and Technology Agency, Tokyo, Japan. [7]Howard Hughes Medical Institute and Department of Molecular Genetics, University of Texas Southwestern Medical Center, Dallas, Texas, USA. [8]Department of Pharmacology, Institute of Basic Medical Sciences, University of Tsukuba, Ibaraki, Japan.

Dialysis dependency is one of the leading causes of morbidity and mortality in the world, and once end-stage renal disease develops, it cannot be reversed by currently available therapy. Although administration of large doses of bone morphogenetic protein–7 (BMP-7) has been shown to repair established renal injury and improve renal function, the pathophysiological role of endogenous BMP-7 and regulatory mechanism of its activities remain elusive. Here we show that the product of *uterine sensitization-associated gene–1* (*USAG1*), a novel BMP antagonist abundantly expressed in the kidney, is the central negative regulator of BMP function in the kidney and that mice lacking USAG-1 (*USAG1*$^{-/-}$ mice) are resistant to renal injury. *USAG1*$^{-/-}$ mice exhibited prolonged survival and preserved renal function in acute and chronic renal injury models. Renal BMP signaling, assessed by phosphorylation of Smad proteins, was significantly enhanced in *USAG1*$^{-/-}$ mice with renal injury, indicating that the preservation of renal function is attributable to enhancement of endogenous BMP signaling. Furthermore, the administration of neutralizing antibody against BMP-7 abolished renoprotection in *USAG1*$^{-/-}$ mice, indicating that USAG-1 plays a critical role in the modulation of renoprotective action of BMP and that inhibition of USAG-1 is a promising means of development of novel treatment for renal diseases.

Introduction

Despite a significant increase in understanding of the pathophysiology of renal diseases, the incidence of end-stage renal disease (ESRD) is still increasing. Tubular damage and interstitial fibrosis are the final common pathway leading to ESRD (1, 2), irrespective of the nature of the initial renal injury, and the degree of tubular damage parallels the impairment of renal function (2). Once tubular damage is established, it cannot be reversed or repaired by currently available treatment, and renal function deteriorates to renal failure, which is often life threatening (3). If we can come up with an agent that can reverse established tubular damage, it would significantly reduce the need for dialysis. Bone morphogenetic protein–7 (BMP-7) is a promising candidate for such an agent, because it is reported to protect the kidney from renal injury (4–8). BMP-7 is known to play essential roles in kidney development, because BMP-7–null mice die shortly after birth due to severe renal hypoplasia (9, 10). BMP-7 is also abundant in the adult kidney, especially in distal tubule epithelial cells (11, 12). Recently, several reports indicated that the expression of BMP-7 is decreased in renal disease models (5, 6, 13–16) and that administration of recombinant BMP-7 at pharmacological doses repairs chronic renal injury (4–8). However, the pathophysiological role and regulatory mechanism of endogenous BMP-7 remain elusive.

The local activity of endogenous BMP is controlled not only by regulation of its expression, but also by certain classes of molecules termed BMP antagonists (17). BMP antagonists function through direct association with BMP, thus inhibiting the binding of BMP to its receptors. *Uterine sensitization-associated gene–1* (*USAG1*) encodes a secreted protein and was initially found as a gene of unknown function whose expression was upregulated in sensitized endometrium of the rat uterus (18). Recently, Avsian-Kretchmer et al. suggested USAG-1 as a candidate for a novel BMP antagonist using bioinformatic analysis (19). Furthermore, Laurikkala et al. demonstrated USAG-1 to be a BMP antagonist expressed in teeth (20).

We independently identified USAG-1 to be a novel BMP antagonist, abundantly expressed in the kidney (21). The expression of USAG-1 is abundant in renal tubules and teeth in late embryogenesis and in adult tissues it is by far most abundant in the kidney, especially in the distal tubule with a pattern similar to that of BMP-7. From these findings, we hypothesized that USAG-1 might regulate the renoprotective action of BMP-7 in the adult kidney.

To evaluate this hypothesis, we generated *USAG1*-knockout (*USAG1*$^{-/-}$) mice and induced acute and chronic renal disease models in which renal tubules, but not glomeruli, were mainly damaged.

Nonstandard abbreviations used: BMP-7, bone morphogenetic protein–7; EMT, epithelial-mesenchymal transition; MCP-1, monocyte chemotactic protein-1; PTEC, proximal tubule epithelial cell; USAG1, uterine sensitization-associated gene–1; UUO, unilateral ureteral obstruction.

Conflict of interest: The authors have declared that no conflict of interest exists.

Citation for this article: *J. Clin. Invest.* **116**:70–79 (2006). doi:10.1172/JCI25445.

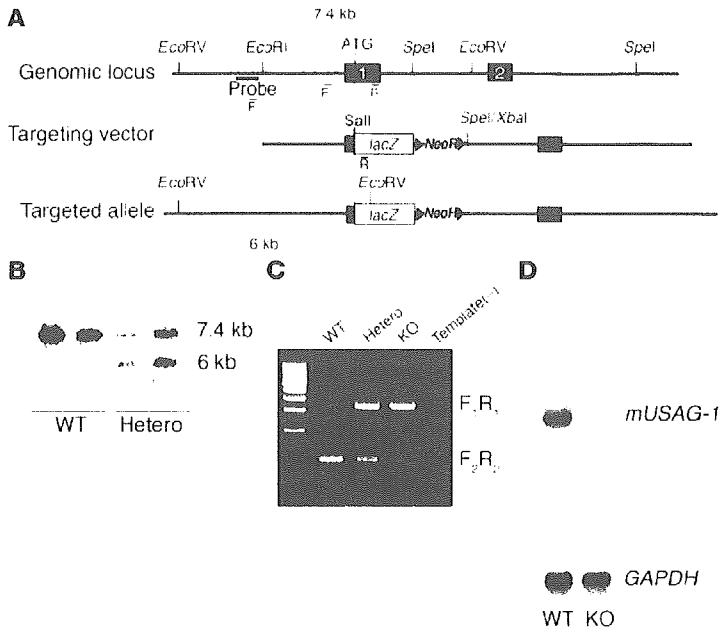

Figure 1
Generation of *USAG1*$^{-/-}$ mutation by gene targeting. (**A**) *USAG1*–null allele was generated by homologous recombination in ES cells. Exon 1 (black box) and part of the intron were replaced with a *lacZ* gene (white box) and the *Neo*R cassette (gray box). (**B**) Analysis of *USAG1*$^{+/+}$ (WT) and correctly targeted heterozygous (Hetero) ES cell clones by Southern blot analysis using 5′ genomic probe (thick black line in **A**). (**C**) PCR genotyping of F_2 littermates. Template(–) is the negative control. (**D**) Northern blot analysis of *USAG1* mRNA in the kidney of *USAG1*$^{+/+}$ and *USAG1*$^{-/-}$ (KO) mice.

Results

Generation and analysis of USAG1$^{-/-}$ *mice.* *USAG1*$^{-/-}$ mice were generated by deleting the first exon including the transcription initiation codon, the signal peptide, and the following 46 amino acids (Figure 1). *USAG1*$^{-/-}$ mice were born at the ratio expected according to Mendel's law of heredity and were viable, fertile, and appeared healthy except that they exhibited supernumerary teeth, both in the incisors and molars, and fused teeth in the molar region (Supplemental Figure 1; supplemental material available online with this article; doi:10.1172/JCI25445DS1). Although there was variation in the sites of extra teeth and fused teeth, this tooth phenotype was fully penetrant. Food consumption was not disturbed by this tooth phenotype in *USAG1*$^{-/-}$ mice (data not shown).

Attenuated acute tubular injury in USAG1$^{-/-}$ *mice.* To induce acute tubular injury, we utilized a cisplatin nephrotoxicity model (22–24). Administration of a nephrotoxic agent, cisplatin, to wild-type littermates caused acute tubular injury that resulted in severe renal failure. Within the first 3 days, 54% of wild-type mice died, while 92% of *USAG1*$^{-/-}$ mice survived the period (Figure 2A). The renal function of *USAG1*$^{-/-}$ mice on day 3 was significantly preserved compared with that in wild-type littermates (Figure 2B). Histological examination of the kidneys of wild-type mice on day 3 showed severe proximal tubular damage, while this change was markedly reduced in *USAG1*$^{-/-}$ mice (Figure 2, C and D). Expression of E-cadherin, a marker for tubular epithelial integrity (25), was markedly reduced in the kidneys of wild-type mice, while its expression was preserved in *USAG1*$^{-/-}$ mice (Figure 2E). Tubular apoptosis, a characteristic feature of tubular injury in cisplatin nephrotoxicity (23), was also significantly reduced in *USAG1*$^{-/-}$ mice (Figure 2F). As reported previously (24), cisplatin administration resulted in upregulation of TNF-α, IL-1β, monocyte chemotactic protein-1 (MCP-1), TGF-β1, and type IV collagen expression in the kidney of wild-type mice. However, the induction of these genes was completely abolished in *USAG1*$^{-/-}$ mice (Figure 2G). Infiltration of macrophages and monocytes in the kidney was also significantly reduced in *USAG1*$^{-/-}$ mice (Figure 2H), in accordance with the reduction of MCP-1 expression (Figure 2G). Expression of BMP-7 was comparable between wild-type mice and *USAG1*$^{-/-}$ mice before and after injection of cisplatin (Figure 2G).

Renal fibrosis is reduced in USAG1$^{-/-}$ *mice.* As a model of chronic renal injury, we performed unilateral ureteral obstruction (UUO) (26, 27) in both *USAG1*$^{-/-}$ mice and wild-type mice, and the kidneys were harvested 14 days after the operation. In wild-type mice, the obstructed kidney showed dilatation/degeneration of renal tubules and interstitial fibrosis, whereas the normal architecture was preserved in *USAG1*$^{-/-}$ mice, except for mild dilatation of tubules (Figure 3, A and B). Expression of E-cadherin was markedly reduced in the kidneys of wild-type mice, while its expression was preserved in *USAG1*$^{-/-}$ mice (Figure 3C). Furthermore, expression of α-SMA, a marker of tubulointerstitial myofibroblasts (28), was upregulated in the interstitium of the obstructed kidney of wild-type mice, while high expression of α-SMA was restricted to vascular smooth muscle cells in *USAG1*$^{-/-}$ mice (Figure 3D). Since expansion and fibrosis of the renal interstitium is another characteristic feature of UUO (6), we examined the deposition of type IV collagen, which is a normal component of the tubular basement membrane. The basement membranes of neighboring tubules are adjacent to each other in the normal kidney. In the obstructed kidney of wild-type mice, expansion of the interstitial component increased the distance between adjacent basement membranes, and type IV collagen produced by interstitial myofibroblasts was aberrantly expressed in the interstitium. However, in the obstructed kidney of *USAG1*$^{-/-}$ mice, the distance between the basement membranes was significantly smaller than that in wild-type mice (Figure 3E). Expression of TNF-α, IL-1β, MCP-1, TGF-β1, and type IV collagen was markedly upregulated on day 14 in the obstructed kidney of wild-type mice. In contrast, the induction of these genes was significantly attenuated, by 33%, 46%, 37%, 75%, and 23%, respectively, in *USAG1*$^{-/-}$ mice (Figure 3F). Expression of BMP-7 in the obstructed kidney was comparable in wild-type mice and *USAG1*$^{-/-}$ mice.

BMP signaling is enhanced in USAG1$^{-/-}$ *mice.* To evaluate whether the reduction in renal injury in *USAG1*$^{-/-}$ mice is attributable to enhanced BMP signaling, phosphorylation of Smad1/5/8 in the kidney was examined in both models (Figure 4). After the induction of kidney disease models, phosphorylation of Smad1/5/8 was hardly detected in wild-type mice, while in *USAG1*$^{-/-}$ mice, the phosphorylation was preserved in the nuclei of tubular epithelial cells (Figure 4A). To examine the specificity of the antibody against phospho-Smad1/5/8, we performed double immunostaining using anti-phospho-Smad1/5/8 antibody and anti-phospho-Smad2/3, and found that most of the nuclei positive for phospho-Smad1/5/8 were negative for phospho-Smad2/3 (Figure 4B), indicating the

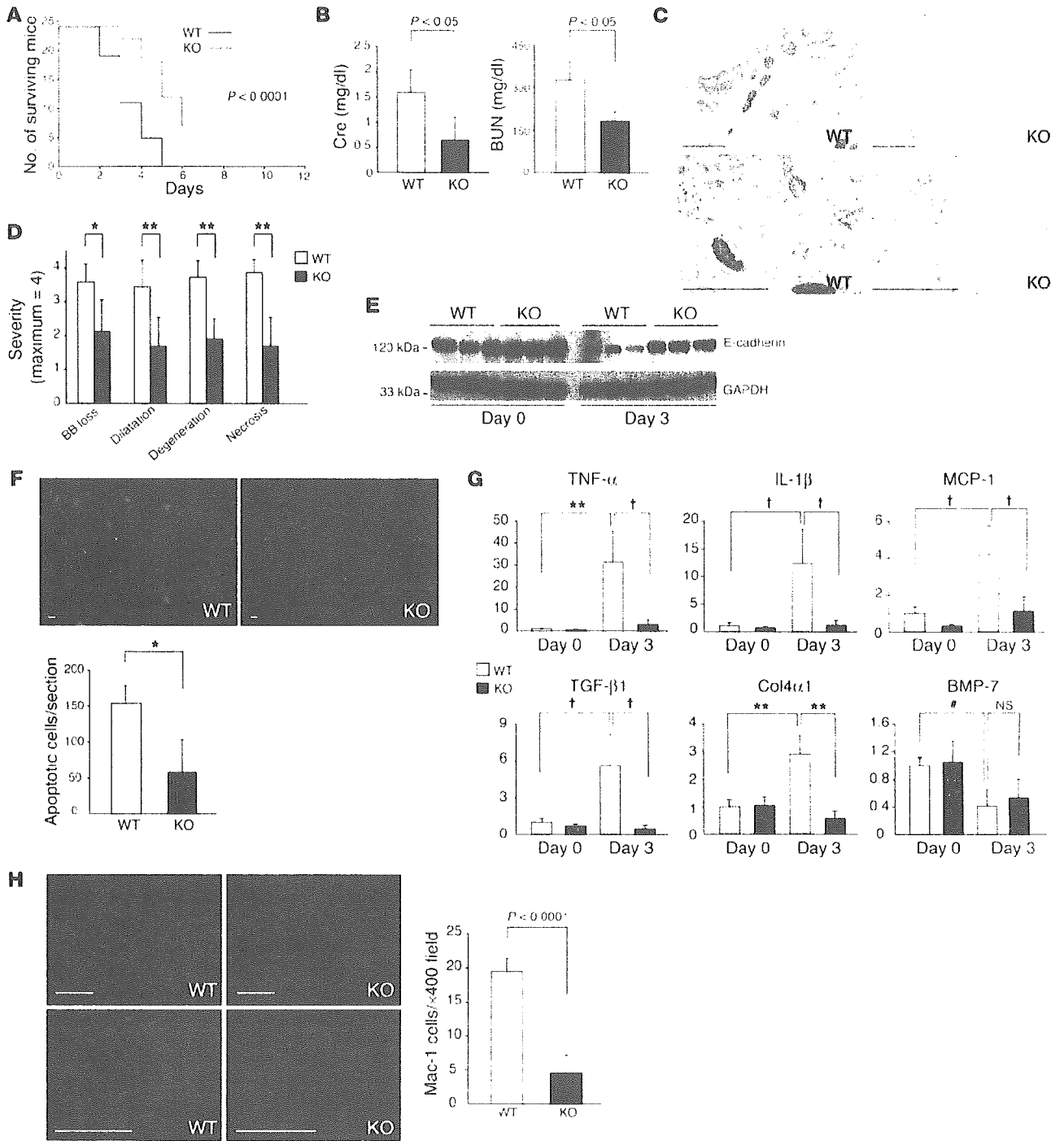

Figure 2

USAG1$^{-/-}$ mice showed less renal injury in cisplatin nephrotoxicity. (**A**) Survival curves of wild-type mice (black line) and *USAG1*$^{-/-}$ mice (red line) after cisplatin administration (n = 24). (**B**) Serum creatinine (Cre) and blood urea nitrogen (BUN) levels at 3 days after injection of cisplatin (n = 6). (**C**) Representative renal histological findings in wild-type mice and *USAG1*$^{-/-}$ mice on day 3. Scale bars: 100 μm. (**D**) Semiquantitative evaluation of morphologic kidney damage, expressed as relative severity on a scale from 0 to 4 (n = 6). Morphological findings were scored according to proximal tubule brush border loss (BB loss), tubule dilatation (Dilatation), tubule degeneration (Degeneration), and tubule necrosis (Necrosis). *P < 0.01; **P < 0.001. (**E**) E-cadherin expression in cisplatin nephrotoxicity. Kidney lysates were subjected to immunoblotting with anti–E-cadherin antibody. Representative data from 4 independent experiments are shown. (**F**) TUNEL staining of kidneys on day 3 of cisplatin nephrotoxicity. The number of TUNEL-positive cells per section was counted in transverse sections (n = 6). Scale bars: 10 μm. (**G**) Gene expression in cisplatin nephrotoxicity. Gene expression was determined by real-time RT-PCR. In each experiment, expression levels were normalized to the expression of GAPDH and expressed relative to mice on day 0. n = 4–6 for each experiment. †P < 0.005; ‡P < 0.02. Col4α1, collagen type IV α 1. (**H**) Infiltration of Mac-1–positive cells after cisplatin injection. The number of Mac-1–positive cells per field was counted in 10 consecutive fields (n = 6). Scale bars: 100 μm.

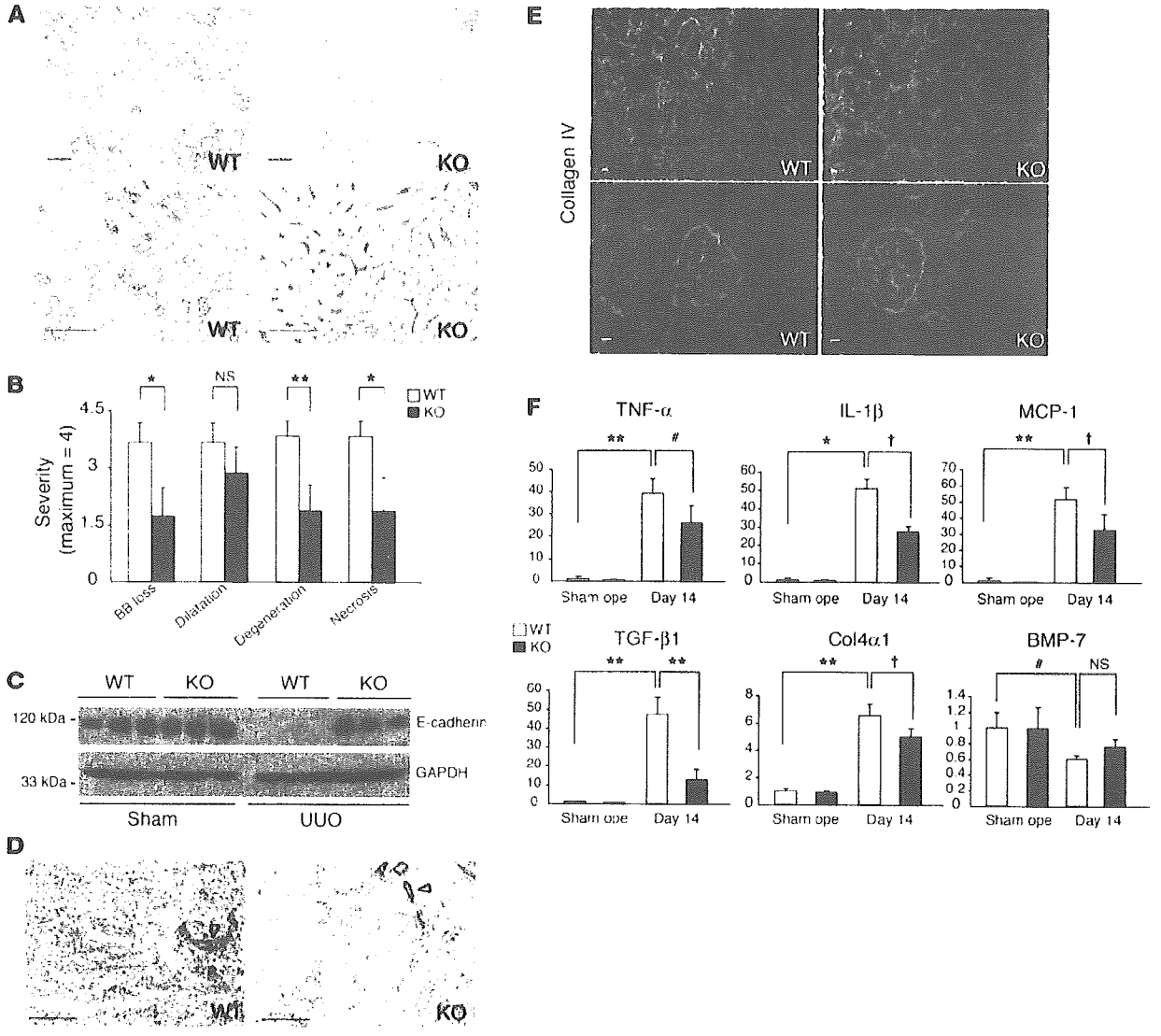

Figure 3

USAG1$^{-/-}$ mice showed reduced EMT and tubulointerstitial fibrosis in UUO. (**A**) Representative histology of the obstructed kidney in wild-type mice and *USAG1*$^{-/-}$ mice 14 days after the operation. Scale bars: 100 μm. (**B**) Semiquantitative evaluation of morphologic kidney damage in wild-type mice and *USAG1*$^{-/-}$ mice, expressed as relative severity on a scale from 0 to 4 (n = 6). (**C**) E-cadherin expression in UUO. Kidney lysates were subjected to immunoblotting with anti–E-cadherin antibody. Representative data from 4 independent experiments are shown. (**D**) Immunostaining of α-SMA in UUO. Arrowheads indicate vascular smooth muscle cells. (**E**) Immunostaining of type IV collagen in UUO. Scale bars: 10 μm. (**F**) Gene expression in UUO. Gene expression was determined by real-time RT-PCR. In each experiment, the expression levels were normalized to the expression of GAPDH and expressed relative to expression in mice on day 0. n = 4–6 for each experiment. $^{\#}P < 0.01$; $^{\dagger}P < 0.005$; $^{*}P < 0.001$; $^{**}P < 0.0001$. Sham ope, mice 14 days after sham operation; day 14, mice 14 days after UUO.

specificity of the antibody against phospho-Smad1/5/8. We also examined the phosphorylation of Smad1/5/8 in immunoblotting of kidney lysates and demonstrated that the phosphorylation was preserved in the kidneys of *USAG1*$^{-/-}$ mice, while it was downregulated in WT mice (Figure 4C). No difference was observed in the phosphorylation of Smad1/5/8 prior to disease induction between *USAG1*$^{-/-}$ mice and WT mice (Figure 4, A and C).

Blocking BMP-7 activity abolishes renoprotection in USAG1$^{-/-}$ *mice.* To analyze the mechanism of renoprotection in *USAG1*$^{-/-}$ mice, we administered a neutralizing antibody against BMP-7 to *USAG1*$^{-/-}$ mice in both kidney disease models. First we evaluated the specificity of the neutralizing activity of the antibody using an assay measuring alkaline phosphatase activity and phosphorylation of Smad1/5/8 in C2C12 cells induced by BMPs. Addition of the antibody inhibited the alkaline phosphatase activity and phosphorylation of Smad1/5/8 induced by BMP-7, but not by BMP-4 (Figure 5A) or BMP-2 (data not shown), indicating the specificity of the antibody. As a negative control, we used isotype-matched IgG2B. Next we administered a neutralizing antibody against BMP-7 to *USAG1*$^{-/-}$ mice with cisplatin nephrotoxicity. Of 7 mice treated with neutralizing antibody, 2 mice died on day 2 and 1 mouse died on day 3, while none of the mice treated with isotype-matched IgG2B

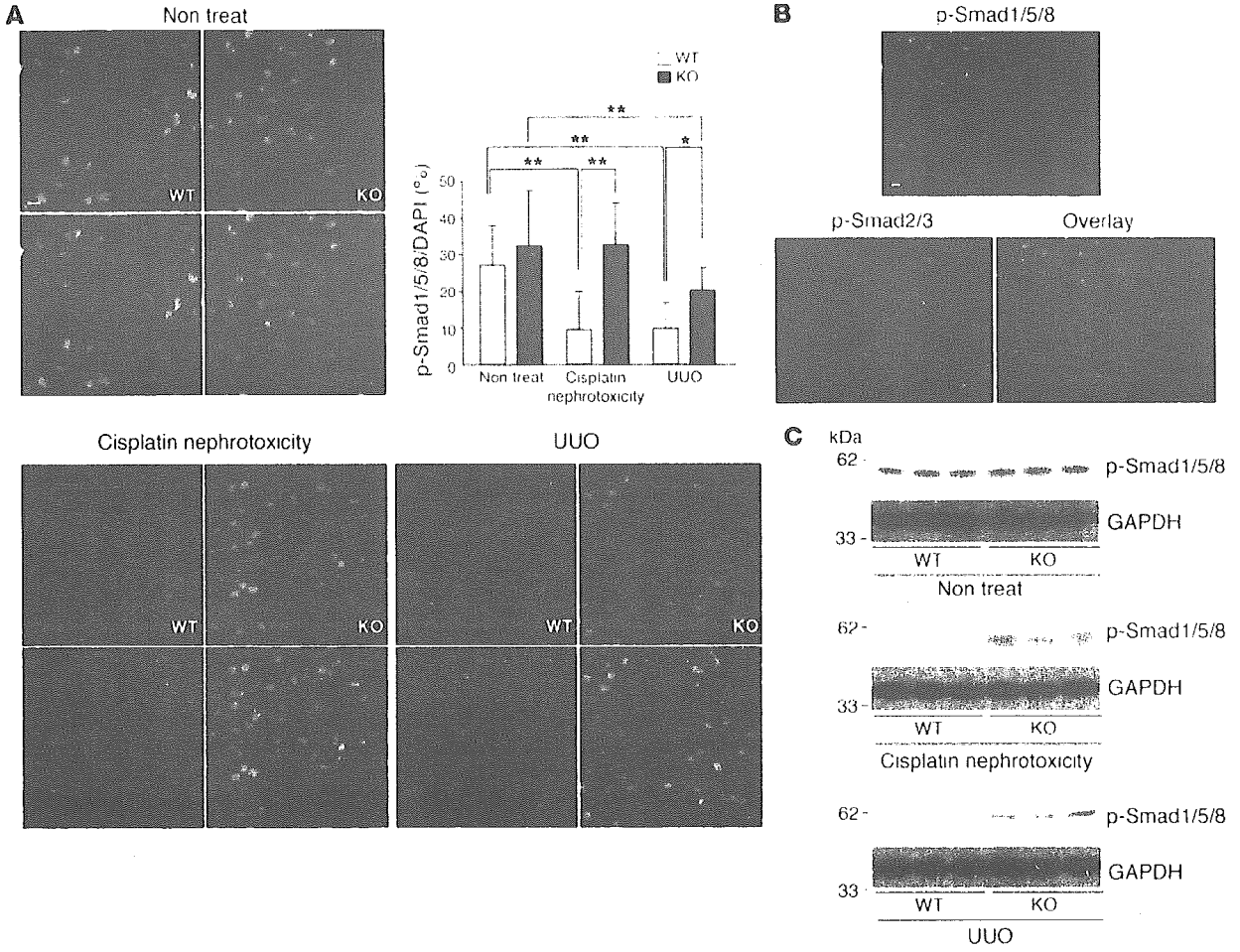

Figure 4
Enhanced BMP signaling in kidneys of *USAG1*$^{-/-}$ mice. (**A**) Phosphorylation of Smad1/5/8 in kidneys of *USAG1*$^{-/-}$ mice and WT mice. The number of pSmad1/5/8-positive nuclei (upper panels) was counted in 10 consecutive fields in each specimen and normalized by the number of DAPI-positive nuclei (lower panels). $n = 6$. Scale bar: 10 μm. $^{*}P < 0.001$; $^{**}P < 0.0001$. Non treat, mice without disease models. (**B**) Double immunostaining of phospho-Smad1/5/8 and phospho-Smad2/3. Almost all the nuclei positive for pSmad1/5/8 were negative for pSmad2/3. Scale bar: 10 μm. (**C**) Immunoblotting of phospho-Smad1/5/8 in kidney lysates prior to disease induction and in both kidney disease models. Representative data from 5 independent experiments are shown.

died within the first 3 days. Administration of neutralizing antibody also resulted in a deterioration of renal function measured by elevation of serum creatinine to a level similar to that in WT mice, while administration of IgG2B did not (Figure 5B). Furthermore, histological examination of the kidneys of *USAG1*$^{-/-}$ mice treated with neutralizing antibody demonstrated severely damaged proximal tubular epithelial cells, while these changes were absent in mice treated with IgG2B (Figure 5B). We also administered the neutralizing antibody to *USAG1*$^{-/-}$ mice with UUO and found that type IV collagen expression in the obstructed kidney was increased in *USAG1*$^{-/-}$ mice treated with neutralizing antibody, but not in those administered IgG2B (Figure 5C). Histological examination of the obstructed kidneys of *USAG1*$^{-/-}$ mice treated with neutralizing antibody demonstrated severe interstitial fibrosis, while this change was almost absent in mice treated with IgG2B (Figure 5C).

USAG1 is the most abundant BMP antagonist in adult kidney. Finally we analyzed the expression of USAG-1 and other BMP antagonists in adult kidneys using modified real-time PCR and in situ hybridization (Figure 6). To compare the expression levels of different genes in real-time PCR, we set the standard curve with the plasmid encoding each BMP antagonist at various concentrations and analyzed the copy number of each gene contained in kidney cDNA. Among known BMP antagonists, USAG-1 was by far the most abundant in the kidneys, and twisted gastrulation was the second most abundant BMP antagonist. We also analyzed the localization of BMP antagonists in the kidneys using in situ hybridization and found that the expression of USAG-1 was confined to distal tubules, as previously described (21), with a pattern similar to that of BMP-7 (12). Expression of twisted gastrulation was also detected in some distal tubules; however, the intensity of the signal was much lower than that of USAG-1, in accordance with the results of real-time PCR. Differential screening selected gene aberrative in neuroblastoma (DAN) and protein related to DAN and Cerberus (PDRC) were faintly observed in the inner medulla, and other BMP antagonists were not detected with this method.

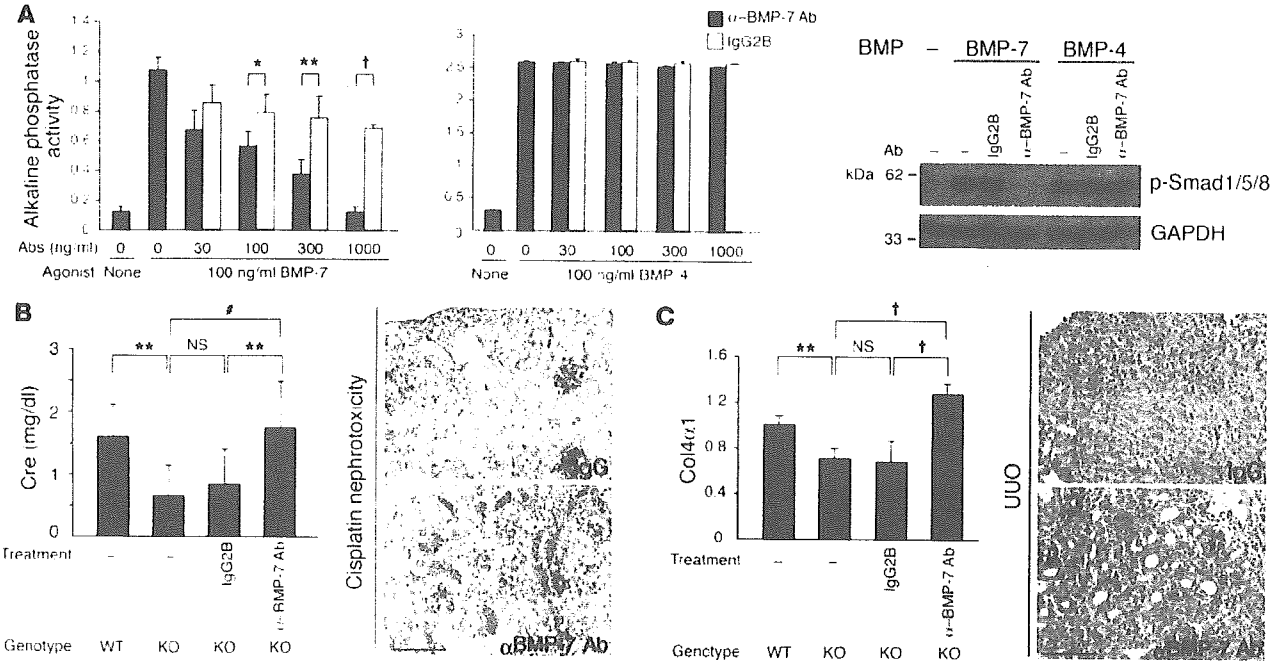

Figure 5

Blocking BMP-7 activity abolishes renoprotection in *USAG1*$^{-/-}$ mice. (**A**) Evaluation of neutralizing activity of anti–BMP-7 antibody. Anti–BMP-7 antibody inhibits alkaline phosphatase activity and phosphorylation of Smad1/5/8 induced by BMP-7, but not by BMP-4. (**B**) Serum creatinine level of *USAG1*$^{-/-}$ mice treated with anti–BMP-7 antibody and representative histological findings on day 3 of cisplatin nephrotoxicity. Scale bar: 100 μm. (**C**) Gene expression of type IV collagen in kidneys of *USAG1*$^{-/-}$ mice treated with anti–BMP-7 antibody and representative histological findings on day 14 of UUO. $^{*}P < 0.1$; $^{**}P < 0.01$; $^{\#}P < 0.001$; $^{\dagger}P < 0.0001$.

Discussion

Epithelial-mesenchymal transition (EMT) is a necessary step for renal fibrosis, as well as in embryonic development and tumor progression (29–31). TGF-β is known to stimulate EMT, while BMP-7 inhibits and reverses the transition (3). Zeisberg et al. recently reported that BMP-7 reverses TGF-β1–induced EMT and induces mesenchymal-epithelial transition in vitro (4, 32). They further demonstrated that administration of a pharmacological dose of BMP-7 resulted in regression of established lesions in the kidney and improved renal function. In this report, we demonstrated that deficiency of USAG-1, a novel BMP antagonist in the kidney, results in marked preservation of renal function by reinforcement of BMP signaling.

Based on these findings, we set the working hypothesis: in many types of renal disease, proximal tubule epithelial cells (PTECs) are the main site of injury (33) and undergo EMT, which causes loss of structural integrity of epithelial cells characterized by a reduction of E-cadherin expression and the induction of α-SMA in interstitial myofibroblasts (Figure 7A). BMP-7 secreted from distal tubules (12) inhibits EMT of PTECs and induces redifferentiation of mesenchymal cells to epithelial cells. USAG-1 produced from distal tubules binds to BMP-7 and inhibits its renoprotective action by interfering with binding to its receptors.

In addition to the inhibition of EMT, many other pharmacological actions of BMP-7 have been reported. Administration of recombinant BMP-7 inhibits the induction of inflammatory cytokine expression in the kidney (12), attenuates inflammatory cell infiltration (6), and reduces apoptosis of tubular epithelial cells in renal disease models (34) (Figure 7A). These phenomena are also observed in *USAG1*$^{-/-}$ mice, and the similarity between BMP-7–treated animals and *USAG1*$^{-/-}$ mice strongly supports our working model that deficiency of USAG-1 reinforces the renoprotective activities of BMP.

In accordance with this hypothesis, the renoprotection in *USAG1*$^{-/-}$ mice was abolished in both renal disease models when a neutralizing antibody against BMP-7 was administered (Figure 5). These results strongly support the hypothesis, and BMP-7 is a potent candidate for the counterpart of USAG-1.

We also observed preserved phosphorylation of Smad1/5/8 in the kidneys of *USAG1*$^{-/-}$ mice in both renal disease models, suggesting that BMP signaling was enhanced in *USAG1*$^{-/-}$ mice, while no difference was observed between WT and KO mice in phosphorylation of Smad1/5/8 prior to disease induction (Figure 4, A and C). We assume that BMP signaling prior to disease induction might be potent enough to cause full phosphorylation of Smad1/5/8 regardless of the presence or absence of USAG-1, while in the later stages of kidney diseases, BMP signaling is decreased and the presence of USAG-1 might cause a further reduction in BMP signaling.

Furthermore, we demonstrated that USAG-1 is by far the most abundant BMP antagonist in the kidney (Figure 6A). Because other BMP antagonists also antagonize BMP-7 activities (Supplemental Figure 2), we conclude that USAG-1 plays an important role in the modulation of BMP activities in the kidney not because of its ligand specificity, but because of its high expression among other BMP antagonists. In addition, the tissue localization of USAG-1 (Figure 6B) is quite similar to that of BMP-7 (12), and USAG-1 can effectively access and inactivate BMP-7 at the site of production.

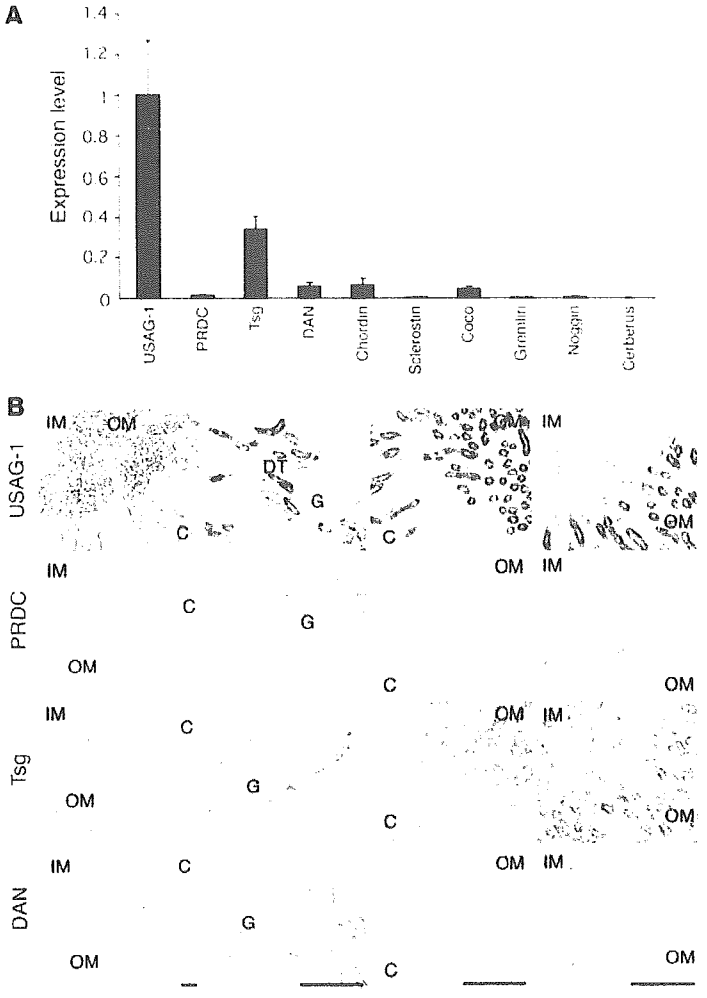

Figure 6

Expression of BMP antagonists in kidney. (**A**) Kidney cDNA of wild-type mice with Svj background was subjected to real-time PCR with various primers for BMP antagonists, and the standard curve was set using the plasmid encoding each BMP antagonist from concentrations of 1 pg/μl to 1 fg/μl. The values of each BMP antagonist in the kidney cDNA were multiplied by the length of the vectors and normalized to the value of USAG-1 expression (n = 4–5). Expression of USAG-1 was by far the most abundant in the kidney among other BMP antagonists. Tsg, twisted gastrulation. (**B**) Kidney sections were subjected to in situ hybridization with probes for all BMP antagonists. Expression of USAG-1 was confined to the distal tubular epithelial cells. Twisted gastrulation was also sparsely expressed in some distal tubules. Differential screening–selected gene aberrative in neuroblastoma (DAN) and protein related to DAN and Cerberus (PDRC) were faintly detected in the inner medulla. Expression of other BMP antagonists was not detected by this method. Scale bars: 100 μm. IM, inner medulla; OM, outer medulla; C, cortex; DT, distal tubule; G, glomerulus.

Although we illustrated USAG-1/BMP-7 binding as occurring outside of PTECs in Figure 7A, it might be possible that the binding occurs intracellularly within the secretory pathway in PTECs and that USAG-1 and BMP-7 are secreted in complex form. Further investigations are necessary to clarify this point.

Interestingly, the expression of USAG-1 decreased during the course of disease models (Supplemental Figure 3 and unpublished observations). We assume that the reduction of USAG-1 in renal diseases is a self-defense mechanism to minimize its inhibitory effect on BMP signaling. Because the reduction in USAG-1 expression in WT mice is not enough to overcome the reduction in BMP-7 expression, further reduction or abolishment of the action of USAG-1 is desirable for the preservation of renal function, and the results of the present study justify therapy targeted toward USAG-1. For example, drugs or neutralizing antibodies that inhibit binding between USAG-1 and BMP or gene-silencing therapy for *USAG1* would enhance the activity of endogenous BMP and might be a promising way to develop novel therapeutic methods for severe renal disease (Figure 7B). Because the expression of USAG-1 is confined to the kidney in adult mice and humans (21), it would be a better target for kidney-specific therapeutic trials. On the other hand, administration of recombinant BMP-7, whose target cells are widely distributed throughout the body, might produce some additional extrarenal actions, including beneficial effects, such as actions on renal osteodystrophy (35–39) and vascular calcification (40, 41).

Furthermore, these therapies targeted toward USAG-1 might protect the kidney during administration of nephrotoxic agents such as cisplatin. The pathological roles of USAG-1 in glomerular injury should be further elucidated before we undertake therapeutic trials against USAG-1.

Despite the essential role of BMP-7 in renal development, we did not observe any developmental abnormality in the kidney of *USAG1* mice with this genetic background. We assume that there are many reasons for the lack of developmental abnormality: First, USAG-1 expression in the developing kidney is not apparent on embryonic day 11.5 (21), whereas BMP-7 expression is intense in the metanephric mesenchyme (42) with a pattern similar to that of gremlin (43). In the later stages, USAG-1 expression appears in the tubular epithelium in the medullary region (21), whereas BMP-7 expression is confined to the condensed mesenchyme and peripheral ureteric epithelium (42). Therefore, the expression pattern of USAG-1 in the developing kidney is totally different from that of BMP-7. Second, the expression of USAG-1 is very low in early embryogenesis, increases toward the late stage of embryogenesis, and is much higher in the adult kidney (21), while the expression of gremlin is high in early embryogenesis with a pattern similar to that of BMP-7, and becomes almost undetectable in the healthy adult kidney (Figure 6). Furthermore, *gremlin*-deficient mice show severe developmental abnormality in the kidney, which is quite similar to that of *BMP-7* deficient mice. Therefore, we conclude that gremlin is a regulator of BMP-7 activity in the developing kidney, and lack of USAG-1 might be compensated by gremlin and does not cause any developmental abnormality in the kidney.

Recently another function of USAG-1 as a modulator of Wnt signaling has been reported in *Xenopus* embryogenesis (44). Although the role of the Wnt pathway in the progression of renal diseases remains to be elucidated, there is a possibility that modulation of the Wnt pathway might also play some roles in the preservation of renal function in *USAG1* mice. Close relationships between the Wnt and BMP pathways have also been reported; for instance, dickkopf homolog 1 (DKK1), a Wnt antagonist, and noggin, a BMP antagonist, cooperate in head induction, while the expression of

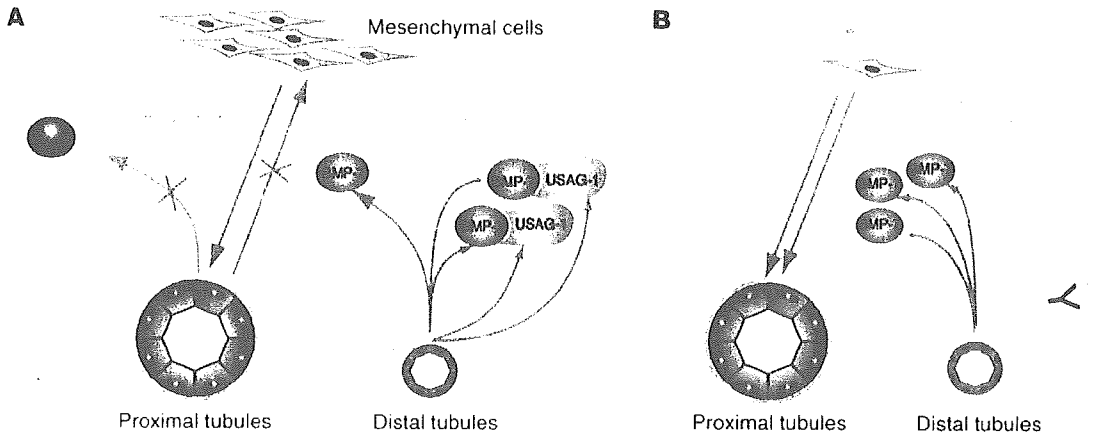

Figure 7
Working model of role of BMP-7 and USAG-1 in renal diseases. (**A**) In renal injury, PTECs are mainly damaged and undergo EMT to fibroblast-like mesenchymal cells. BMP-7 secreted by the distal tubule inhibits EMT and apoptosis of PTECs. USAG-1 is also secreted by the distal tubule, binds to BMP-7, and inhibits the renoprotective actions of BMP-7. (**B**) Therapeutic implication of USAG-1. Reduction of USAG-1 activity, for example, by a neutralizing antibody blocking the binding of USAG-1 and BMP-7, results in reinforcement of the renoprotective action of BMP-7. MET, mesenchymal-epithelial transition.

DKK1 is regulated by BMP-4 in limb development. Furthermore, a BMP antagonist, cerberus, has binding sites for both Wnt and BMP and antagonizes the activities of both the Wnt and BMP signaling pathways. USAG-1 might also have dual activities and act as a molecular link between these 2 important signaling pathways.

In conclusion, this study showed that USAG-1 plays important roles in the progression of renal diseases and might be a potent negative regulator of the renoprotective action of endogenous BMP signaling. Recently, Lin et al. identified a positive regulator of BMP-7 named kielin/chordin-like protein (KCP) and demonstrated that *KCP*$^{-/-}$ mice are susceptible to tubular injury and interstitial fibrosis (45). These data support the idea that BMP-7 protects the kidney from renal injury. Because these negative and positive modulators of BMP signaling regulate and edge the boundaries of BMP activity, further understanding of these modulators would give valuable information about their pathophysiological functions and provide a rationale for a therapeutic approach against these proteins.

Methods

Generation of USAG1$^{-/-}$ *mice.* We isolated a genomic fragment containing the mouse *USAG1* gene by screening a 129/SvJ genomic library (Stratagene). We inserted an *nlacZ* gene and a PGK-*Neo*R cassette in the opposite transcriptional orientation to the *USAG1* gene. ES cells were transfected with the linearized targeting vector by electroporation and selected by G418-containing medium. Homologous recombinants were screened and identified by genomic Southern blot analysis with an *Hin*cII-*Eco*RI probe mapping outside the 5′ homology arm (Figure 1A). Homologous recombined ES cell clones were obtained, and correct recombination was confirmed by Southern blot (Figure 1B) as well as PCR analyses. ES cells carrying the *USAG1*-null allele were injected into C57BL/6 blastocysts to obtain chimeric mice, which were crossed with wild-type C57BL/6J mice. Following germline transmission, the mice were maintained in a mixed SvJ background. PCR genotyping was used for all subsequent studies to allow specific detection of both the wild-type and *USAG1*$^{-/-}$ alleles (Figure 1C). Sequences of the primers used for genotyping are as follows: F1, CCCCTCCTCATCTGGCTGCTTCCTAAACGG; R1, CAGTCACGACGTTGTAAAACGACGGGATCC; F2, GGGATCCCACCCCTTCTCT; and R2, GCCGGGACAGGTTTAACCA.

Animal use. All experiments except those represented in Supplemental Figure 3 were performed using *USAG1*$^{-/-}$ mice and their wild-type littermates (*USAG1*$^{+/+}$) of the F_2 generation. All mice were housed in specific pathogen-

Table 1
Primers for real-time RT-PCR

Gene	Sequence of primers (5′-3′)
GAPDH	CCAGAACATCATCCCTGCATC; CCTGCTTCACCACCTTCTTGA
TNFα	ATGAGAAGTTCCCAAATGGCC; CCTCCACTTGGTGGTTTGCTA
IL-1β	CCTTCCAGGATGAGGACATGA; AACGTCACACACCAGCAGGTT
TGFβ1	GCAACAATTCCTGGCGTTACC; CGAAAGCCCTGTATTCCGTCT
MCP-1	TGCATCTGCCCTAAGGTCTTC; AAGTGCTTGAGGTGGTTGTGG
Col4α1	TTCCTTCGTGATGCACACCA; TTCTCATGCACACTTGGCAGC
USAG1	GCAACAGCACCCTGAATCAAG; TGTATTTGGTGGACCGCAGTT
Chordin	GCAGTGGTTCCCAGAGAATCA; AACAATCGTCCCGCTCACAGT
DAN	CTTCAGTTACAGCGTCCCCAA; CCAAGGTCACAATCTCCCACA
PRDC	AGGAGGCTTCCATCTCGTCAT; CCGGTTCTTCCGTGTTTCA
Twisted gastrulation	AAACGTGTCTGTTCCCAGCAA; ACACTGGTGGATGGACATGCA
Gremlin	AGCCCAAGAAGTTCACCACCA; TATGCAACGGCACTGCTTCAC
Sclerostin	CAAGCCTTCAGGAATGATGCC; TCGGACACATCTTTGGCGT
Noggin	AGAAACAGCGCCTGAGCAAGA; AAAAGCGGCTGCCTAGGTCAT
Cerberus	CCCATCAAAAGCCACGAAGT; CCAAAGCAAAGGTTGTTCTGG
Coco	TCCGCTTTTAGCCACTAGGTG; GCTGTTATTCTGGTGTCCCCA
BMP-2	TCGACCATGGTGGCCGGGACCCG; TGTTCCCGGAAGATCTGGAGT
BMP-3	AGCGAATGGATTATCTCTCCCA; TCTTTTCCGGCACACAGCA
BMP-4	CTGGAATGATTGGATTGTGGC; GCATGGTTGGTTGAGTTGAGG
BMP-5	AAGCCTGCAAGAAGCACGAA; GGAAAAGAACATTCCCCGTCA
BMP-6	CCAACCACGCCATTGTACAGA; GGAATCCAAGGCAGAACCATG
BMP-7	TGTGGCAGAAAACAGCAGCA; TCAGGTGCAATGATCCAGTCC

free conditions. Experiments represented in Supplemental Figure 3 were performed using C57BL/6 mice. All animal experiments were approved by the Animal Research Committee at the Graduate School of Medicine, Kyoto University, and the Animal Experiment and Use Committee at the University of Tsukuba and were in accordance with NIH guidelines.

Cisplatin administration. Cisplatin (Sigma-Aldrich) was administered at 20 mg/kg to mice by a single intraperitoneal injection. Mice were sacrificed 72 hours after administration of cisplatin, and tissue and blood were collected for further analysis.

UUO. Complete UUO was performed as previously described (46). Briefly, under sodium pentobarbital anesthesia, the middle portion of the left ureter was ligated and cut between 2 ligated points. At 14 days after surgery, the mice were sacrificed, and the obstructed kidneys were subjected to the studies described below.

Histological studies. The kidneys were fixed in Carnoy solution and embedded in paraffin. Sections (2 μm) were stained with PAS for routine histological examination, and the degree of morphological changes was determined using light microscopy. The following parameters were chosen as indicative of morphological damage to the kidney after cisplatin injection and UUO: brush border loss, tubule dilatation, tubule degeneration, and tubule necrosis. These parameters were evaluated on a scale of 0 to 4, and classed as: 0, not present; 1, mild; 2, moderate; 3, severe; and 4, very severe. The remaining kidney was used for immunohistochemical study, RNA isolation, and protein extraction.

Immunostaining. Frozen sections of kidneys were subjected to immunostaining with polyclonal antibodies against type IV collagen (ICN Pharmaceuticals), phosphorylated Smad1/5/8 (Cell Signaling Technology), and phosphorylated Smad2/3 (Santa Cruz Biotechnology Inc.) and monoclonal antibodies against α-SMA (Sigma-Aldrich) and Mac-1 (BD Biosciences — Pharmingen) as previously described (47, 48).

Immunoblotting. Whole kidney protein was homogenized in RIPA buffer (50 mM Tris at pH 7.5, 150 mM NaCl, 1% Nonidet P-40, 0.25% SDS, 1 mM Na_3VO_4, 2 mM EDTA, 1 mM PMSF, and 10 μg/ml aprotinin) and subjected to immunoblotting as described previously (49). Anti-E-cadherin antibody and anti-GAPDH antibody were from BD Biosciences — Transduction Laboratories and Research Diagnostic Inc., respectively.

Apoptosis detection and quantification. The TUNEL technique (In Situ Cell Death Detection Kit; Roche Diagnostics GmbH) was used to detect apoptotic cells in situ. All apoptotic nuclei within a transverse section at the renal pelvis were counted.

Quantification of mRNA by real-time RT-PCR. Real-time RT-PCR was performed with a 7700 Sequence Detection System (Applied Biosystems). Five micrograms of total RNA was reverse transcribed in a reaction volume of 20 μl using Superscript III reverse transcriptase and random primers (Invitrogen Corp.). The product was diluted to a volume of 400 μl, and 5-μl aliquots were used as templates for amplification using SYBR Green PCR amplification reagent (Applied Biosystems) and gene-specific primers. Specific primers for each gene transcript (listed in Table 1) were designed using Primer Express software version 2.0.0 (Applied Biosystems) and checked as to whether they showed a single peak in the dissociation curve. Serially diluted cDNA or plasmids encoding probes for in situ hybridization were used to generate the standard curve for each primer, and the PCR conditions were as follows: 50°C for 2 minutes, 95°C for 10 minutes, then 95°C for 15 seconds and 60°C for 1 minute for 40 cycles.

Administration of neutralizing antibody against BMP-7. In cisplatin nephrotoxicity, 1.5 mg/kg neutralizing anti–BMP-7 antibody (R&D Systems Inc.) was peritoneally injected into *USAG1*$^{-/-}$ mice 24 hours after injection of cisplatin. In UUO, 0.5 mg/kg neutralizing anti–BMP-7 antibody was injected every 3 days from day 2 to day 11. As a negative control, isotype-matched IgG2B (BD Biosciences) was injected at the same time points. Neutralizing activity of the antibody was evaluated by an assay measuring the production of alkaline phosphatase activity by C2C12 cells, as previously described (21).

In situ hybridization. The kidneys were excised from adult male mice and fixed in 4% paraformaldehyde in PBS. Frozen sections (5 μm thick) were treated with 1 μg/ml proteinase K in PBS at 37°C for 30 minutes and acetylated in 0.1 M triethanolamine-HCl, 0.25% acetic anhydride for 15 minutes. Hybridization was performed with probes at concentrations of about 1 μg/ml in a hybridization solution (50% formamide, ×5 SSC, 1% SDS, 50 μg/ml transfer RNA, and 50 μg/ml heparin) at 60°C for 16 hours. RNA probes were synthesized by in vitro transcription with a DIG RNA Labeling Mix (Roche Diagnostics Corp.). Each probe was designed to contain an open reading frame with the following length and G+C content: USAG-1, 1.0 kbp (G+C 52.6%); sclerostin, 1.5 kbp (61.7%); coco, 1.2 kbp (54.7%); DAN, 1.0 kbp (60.6%); twisted gastrulation, 0.7 kbp (55.1%); PRDC, 0.8 kbp (57.7%); chordin, 1.5 kbp (60.2%); gremlin, 0.9 kbp (50%); noggin, 0.7 kbp (64.7%); cerberus, 1.5 kbp (48.8%). Hybridization was detected using an anti-DIG AP conjugate (Roche Diagnostic Corp.) and NBT/BCIP solution (Roche Diagnostics Corp.).

Analysis of phenotype of adult teeth. Skeletal preparations of the maxillae and mandibles were made by soaking the mouse heads in 0.02% proteinase K in PBS at 37°C for 4 days after peeling off the skin, dissecting the maxillae and mandibles, and clearing them in 5% H_2O_2 at room temperature for 5 minutes. Finally they were rinsed in H_2O and left to dry.

Statistics. All assays were performed in triplicate. Data are presented as mean ± SD. Statistical significance was assessed by ANOVA, followed by Fisher's protected least significant difference post-hoc test. Survival curves were derived using the Kaplan-Meier method and compared using log-rank test.

Acknowledgments

We are grateful to Y. Nabeshima, T. Nakahata, and T. Nakamura for helpful discussion. We are grateful to M. Yoshimoto for hematological evaluation of the mice. We thank A. Ooda, H. Uchiyama, and A. Hosoya for technical assistance. We thank W. Gray for reading the manuscript.

Received for publication April 25, 2005, and accepted in revised form October 11, 2005.

Address correspondence to: Motoko Yanagita, COE Formation for Genomic Analysis of Disease Model Animals with Multiple Genetic Alterations, Graduate School of Medicine, Kyoto University, Shogoin Kawahara-cho 54, Kyoto 606-8507, Japan. Phone: 81-75-751-3465; Fax: 81-75-751-3574; E-mail: motoy@kuhp.kyoto-u.ac.jp.

1. Eddy, A.A. 1996. Molecular insights into renal interstitial fibrosis. *J. Am. Soc. Nephrol.* **7**:2495–2508.
2. van Kooten, C., Daha, M.R., and van Es, L.A. 1999. Tubular epithelial cells: a critical cell type in the regulation of renal inflammatory processes. *Exp. Nephrol.* **7**:429–437.
3. Neilson, E.G. 2005. Setting a trap for tissue fibrosis. *Nat. Med.* **11**:373–374.
4. Zeisberg, M., et al. 2003. BMP-7 counteracts TGF-beta1-induced epithelial-to-mesenchymal transition and reverses chronic renal injury. *Nat. Med.* **9**:964–968.
5. Vukicevic, S., et al. 1998. Osteogenic protein-1 (bone morphogenetic protein-7) reduces severity of injury after ischemic acute renal failure in rat. *J. Clin. Invest.* **102**:202–214.
6. Hruska, K.A., et al. 2000. Osteogenic protein-1 prevents renal fibrogenesis associated with ureteral obstruction. *Am. J. Physiol. Renal Physiol.* **279**:F130–F143.
7. Hruska, K.A. 2002. Treatment of chronic tubulointerstitial disease: a new concept. *Kidney Int.* **61**:1911–1922.
8. Zeisberg, M., et al. 2003. Bone morphogenic protein-7 inhibits progression of chronic renal fibrosis associated with two genetic mouse models. *Am. J. Physiol. Renal Physiol.* **285**:F1060–F1067.

9. Dudley, A.T., Lyons, K.M., and Robertson, E.J. 1995. A requirement for bone morphogenetic protein-7 during development of the mammalian kidney and eye. *Genes Dev.* **9**:2795–2807.
10. Luo, G., et al. 1995. BMP-7 is an inducer of nephrogenesis, and is also required for eye development and skeletal patterning. *Genes Dev.* **9**:2808–2820.
11. Ozkaynak, E., et al. 1990. OP-1 cDNA encodes an osteogenic protein in the TGF-beta family. *EMBO J.* **9**:2085–2093.
12. Gould, S.E., Day, M., Jones, S.S., and Dorai, H. 2002. BMP-7 regulates chemokine, cytokine, and hemodynamic gene expression in proximal tubule cells. *Kidney Int.* **61**:51–60.
13. Simon, M., et al. 1999. Expression of bone morphogenetic protein-7 mRNA in normal and ischemic adult rat kidney. *Am. J. Physiol.* **276**:F382–F389.
14. Wang, S.N., Lapage, J., and Hirschberg, R. 2001. Loss of tubular bone morphogenetic protein-7 in diabetic nephropathy. *J. Am. Soc. Nephrol.* **12**:2392–2399.
15. Lund, R.J., Davies, M.R., and Hruska, K.A. 2002. Bone morphogenetic protein-7: an anti-fibrotic morphogenetic protein with therapeutic importance in renal disease. *Curr. Opin. Nephrol. Hypertens.* **11**:31–36.
16. Almanzar, M.M., et al. 1998. Osteogenic protein-1 mRNA expression is selectively modulated after acute ischemic renal injury. *J. Am. Soc. Nephrol.* **9**:1456–1463.
17. Massague, J., and Chen, Y.G. 2000. Controlling TGF-beta signaling. *Genes Dev.* **14**:627–644.
18. Simmons, D.G., and Kennedy, T.G. 2002. Uterine sensitization-associated gene-1: a novel gene induced within the rat endometrium at the time of uterine receptivity/sensitization for the decidual cell reaction. *Biol. Reprod.* **67**:1638–1645.
19. Avsian-Kretchmer, O., and Hsueh, A.J. 2004. Comparative genomic analysis of the eight-membered ring cystine knot-containing bone morphogenetic protein antagonists. *Mol. Endocrinol.* **18**:1–12.
20. Laurikkala, J., Kassai, Y., Pakkasjarvi, L., Thesleff, I., and Itoh, N. 2003. Identification of a secreted BMP antagonist, ectodin, integrating BMP, FGF, and SHH signals from the tooth enamel knot. *Dev. Biol.* **264**:91–105.
21. Yanagita, M., et al. 2004. USAG-1: a bone morphogenetic protein antagonist abundantly expressed in the kidney. *Biochem. Biophys. Res. Commun.* **316**:490–500.
22. Schrier, R.W. 2002. Cancer therapy and renal injury. *J. Clin. Invest.* **110**:743–745. doi:10.1172/JCI200216568.
23. Megyesi, J., Safirstein, R.L., and Price, P.M. 1998. Induction of p21WAF1/CIP1/SDI1 in kidney tubule cells affects the course of cisplatin-induced acute renal failure. *J. Clin. Invest.* **101**:777–782.
24. Ramesh, G., and Reeves, W.B. 2002. TNF-α mediates chemokine and cytokine expression and renal injury in cisplatin nephrotoxicity. *J. Clin. Invest.* **110**:835–842. doi:10.1172/JCI200215606.
25. Yang, J., and Liu, Y. 2001. Dissection of key events in tubular epithelial to myofibroblast transition and its implications in renal interstitial fibrosis. *Am. J. Pathol.* **159**:1465–1475.
26. Klahr, S., and Morrissey, J. 2002. Obstructive nephropathy and renal fibrosis. *Am. J. Physiol. Renal Physiol.* **283**:F861–F875.
27. Chevalier, R.L. 1999. Molecular and cellular pathophysiology of obstructive nephropathy. *Pediatr. Nephrol.* **13**:612–619.
28. Sato, M., Muragaki, Y., Saika, S., Roberts, A.B., and Ooshima, A. 2003. Targeted disruption of TGF-beta1/Smad3 signaling protects against renal tubulointerstitial fibrosis induced by unilateral ureteral obstruction. *J. Clin. Invest.* **112**:1486–1494. doi:10.1172/JCI200319270.
29. Kalluri, R., and Neilson, E.G. 2003. Epithelial-mesenchymal transition and its implications for fibrosis. *J. Clin. Invest.* **112**:1776–1784. doi:10.1172/JCI200320530.
30. Bottinger, E.P., and Bitzer, M. 2002. TGF-beta signaling in renal disease. *J. Am. Soc. Nephrol.* **13**:2600–2610.
31. Iwano, M., et al. 2002. Evidence that fibroblasts derive from epithelium during tissue fibrosis. *J. Clin. Invest.* **110**:341–350. doi:10.1172/JCI200215518.
32. Zeisberg, M., Shah, A.A., and Kalluri, R. 2005. Bone morphogenic protein-7 induces mesenchymal to epithelial transition in adult renal fibroblasts and facilitates regeneration of injured kidney. *J. Biol. Chem.* **280**:8094–8100.
33. Gerritsma, J.S., van Kooten, C., Gerritsen, A.F., van Es, L.A., and Daha, M.R. 1998. Transforming growth factor-beta 1 regulates chemokine and complement production by human proximal tubular epithelial cells. *Kidney Int.* **53**:609–616.
34. Li, T., Surendran, K., Zawaideh, M.A., Mathew, S., and Hruska, K.A. 2004. Bone morphogenetic protein 7: a novel treatment for chronic renal and bone disease. *Curr. Opin. Nephrol. Hypertens.* **13**:417–422.
35. Davies, M.R., Lund, R.J., Mathew, S., and Hruska, K.A. 2005. Low turnover osteodystrophy and vascular calcification are amenable to skeletal anabolism in an animal model of chronic kidney disease and the metabolic syndrome. *J. Am. Soc. Nephrol.* **16**:917–928.
36. Gonzalez, E.A., et al. 2002. Treatment of a murine model of high-turnover renal osteodystrophy by exogenous BMP-7. *Kidney Int.* **61**:1322–1331.
37. Hruska, K.A., et al. 2004. Kidney-bone, bone-kidney, and cell-cell communications in renal osteodystrophy. *Semin. Nephrol.* **24**:25–38.
38. Lund, R.J., Davies, M.R., Brown, A.J., and Hruska, K.A. 2004. Successful treatment of an adynamic bone disorder with bone morphogenetic protein-7 in a renal ablation model. *J. Am. Soc. Nephrol.* **15**:359–369.
39. Simic, P., and Vukicevic, S. 2005. Bone morphogenetic proteins in development and homeostasis of kidney. *Cytokine Growth Factor Rev.* **16**:299–308.
40. Davies, M.R., Lund, R.J., and Hruska, K.A. 2003. BMP-7 is an efficacious treatment of vascular calcification in a murine model of atherosclerosis and chronic renal failure. *J. Am. Soc. Nephrol.* **14**:1559–1567.
41. Hruska, K.A., Mathew, S., and Saab, G. 2005. Bone morphogenetic proteins in vascular calcification. *Circ. Res.* **97**:105–114.
42. Godin, R.E., Takaesu, N.T., Robertson, E.J., and Dudley, A.T. 1998. Regulation of BMP7 expression during kidney development. *Development.* **125**:3473–3482.
43. Michos, O., et al. 2004. Gremlin-mediated BMP antagonism induces the epithelial-mesenchymal feedback signaling controlling metanephric kidney and limb organogenesis. *Development.* **131**:3401–3410.
44. Itasaki, N., et al. 2003. Wise, a context-dependent activator and inhibitor of Wnt signalling. *Development.* **130**:4295–4305.
45. Lin, J., et al. 2005. Kielin/chordin-like protein, a novel enhancer of BMP signaling, attenuates renal fibrotic disease. *Nat. Med.* **11**:387–393.
46. Nishida, M., et al. 2002. Absence of angiotensin II type 1 receptor in bone marrow-derived cells is detrimental in the evolution of renal fibrosis. *J. Clin. Invest.* **110**:1859–1868. doi:10.1172/JCI200215045.
47. Yanagita, M., et al. 2001. Gas6 regulates mesangial cell proliferation through Axl in experimental glomerulonephritis. *Am. J. Pathol.* **158**:1423–1432.
48. Yanagita, M., et al. 2001. Gas6 induces mesangial cell proliferation via latent transcription factor STAT3. *J. Biol. Chem.* **276**:42364–42369.
49. Yanagita, M., et al. 2002. Essential role of Gas6 for glomerular injury in nephrotoxic nephritis. *J. Clin. Invest.* **110**:239–246. doi:10.1172/JCI200214861.

Am J Physiol Heart Circ Physiol 290: H709–H715, 2006.
First published September 23, 2005; doi:10.1152/ajpheart.00186.2005.

Activation of TGF-β1-TAK1-p38 MAPK pathway in spared cardiomyocytes is involved in left ventricular remodeling after myocardial infarction in rats

Madoka Matsumoto-Ida,* Yoshihito Takimoto,* Takeshi Aoyama, Masaharu Akao, Toshihiro Takeda, and Toru Kita

Department of Cardiovascular Medicine, Kyoto University Graduate School of Medicine, Kyoto, Japan

Submitted 25 February 2005; accepted in final form 19 September 2005

Matsumoto-Ida, Madoka, Yoshihito Takimoto, Takeshi Aoyama, Masaharu Akao, Toshihiro Takeda, and Toru Kita. Activation of TGF-β1-TAK1-p38 MAPK pathway in spared cardiomyocytes is involved in left ventricular remodeling after myocardial infarction in rats. *Am J Physiol Heart Circ Physiol* 290: H709–H715, 2006. First published September 23, 2005; doi:10.1152/ajpheart.00186.2005.—Transforming growth factor-β1 (TGF-β1) alters myocardial gene expression, resulting in myocyte hypertrophy, through activation of TGF-β-activated kinase (TAK1), a member of the mitogen-activated protein kinase kinase kinase (MAPKKK) family. We hypothesized that the TGF-β1-TAK1-p38 MAPK pathway might be activated during ventricular remodeling after myocardial infarction (MI). One, 3, 7, and 14 days after ligation of the left anterior descending coronary artery, noninfarcted left ventricular tissue samples were obtained. Protein levels as well as mRNA levels of the signaling pathway, TGF-β1, TGF-β-receptors, and TAK1 increased in the noninfarcted myocardium in MI rats compared with sham-operated animals. Phosphorylation of MAPKK 3/6 (MKK3/6) and p38 MAPK, the downstream targets of TAK1, was also increased in the noninfarcted region. Moreover, an in vitro kinase assay revealed that the activated TAK1 in the noninfarcted myocardium was capable of activating recombinant MKK3/6, suggesting a causative role of TAK1 in the remodeling process. The activation of the TGF-β1-TAK1-p38 MAPK pathway paralleled the transcriptional upregulation of cardiac markers for ventricular hypertrophy, β-myosin heavy chain and atrial natriuretic peptide. TAK1 was mainly localized to cardiomyocytes, whereas TGF-β1 receptors were observed in vascular smooth muscle cells and fibroblasts as well as cardiomyocytes. Thus the TGF-β1-TAK1-MKK3/6-p38 MAPK pathway in the cardiomyocytes of noninfarcted spared myocardium is activated after acute MI and may play an important role in ventricular hypertrophy and post-MI remodeling in rats.

signal transduction; cytokine; hypertrophy; transforming growth factor-β1-activated kinase; mitogen-activated protein kinase

CARDIAC REMODELING refers to the process by which the normal cardiac architecture is altered in response to myocardial infarction (MI) (4, 16, 23, 24). Although remodeling is an adaptive mechanism against increased wall stresses, it also contributes to the progression of heart failure; decreased ventricular compliance contributes to diastolic dysfunction, which over time is followed by the development of progressive contractile dysfunction. Microscopically, remodeling is featured by hypertrophic growth of cardiomyocytes and hyperplastic growth of cardiac fibroblasts, as well as wound healing in the scar. These histological changes are based on various alterations of genetic expression: the reexpression of a "fetal" gene program, including the upregulation of genes such as β-myosin heavy chain (β-MHC) and atrial natriuretic peptide (ANP) (19, 22).

Inflammatory cytokines play pivotal roles in post-MI left ventricular remodeling (12). Among them, transforming growth factor (TGF)-β1 is upregulated after MI (3, 27, 29) and constitutes the signaling network with the renin-angiotensin system to promote cardiac remodeling (17). TGF-β1 causes the induction of fetal gene expression in cardiomyocytes and stimulates the production of extracellular matrix protein by cardiac fibroblasts (6, 15, 17). TGF-β1 elicits its biological responses through a heteromeric receptor complex comprising two serine-threonine kinase receptors, termed TGF-β receptor types I and II (TβRI and TβRII) (10). The signal is transduced to a member of the MAPK kinase kinase (MAPKKK) family, TGF-β-activated kinase (TAK1), which subsequently activates MKK3/6 (MAPKK) and p38 MAPK (30). Zhang et al. (32) reported that an activating mutation of TAK1 expressed in myocardium of transgenic mice produced p38 MAPK phosphorylation in vivo, cardiac hypertrophy, interstitial fibrosis, severe myocardial dysfunction, "fetal" gene induction, apoptosis, and early lethality. However, the role of TAK1 in post-MI remodeling remains to be determined.

Therefore we hypothesized that the TGF-β1-TAK1-MKK3/6-p38 MAPK pathway may be activated during ventricular remodeling after MI. We examined the protein levels of these peptides, their localizations, and the correlation between this pathway and ventricular remodeling, using a rat model of MI.

MATERIALS AND METHODS

Animals with MI. We performed animal experiments in accordance with the Declaration of Helsinki, and these were approved by our institutional ethics committee for animal experiments.

MI was surgically induced in 8-wk-old male Sprague-Dawley rats (Charles River Japan, Yokohama, Japan) weighing 280–320 g by ligation of the left anterior descending coronary artery, as described previously (1, 26). In brief, the chest was opened via an anterior thoracotomy, and the heart was rapidly exteriorized. The proximal left anterior descending coronary artery was ligated about 2 mm distal to its aortic origin with a 7-0 silk suture. Successful ligation was confirmed by regional cyanosis of the myocardial surface. The heart was returned to its original position, and the incision was closed. Sham-operated animals underwent identical surgery except for the coronary artery ligation. After the operation, rats were allowed free access to standard rat chow, and water was provided ad libitum.

The overall mortality of MI rats during the entire experimental period (up to 14 days after MI) was 30–40%. The majority of death occurred on the day or the following day of the MI surgery, probably

* M. Matsumoto-Ida and Y. Takimoto contributed equally to this work.

Address for reprint requests and other correspondence: T. Aoyama, Kansai Electric Power Hospital, 2-1-7 Fukushima, Fukushima-ku, Osaka 553-0003, Japan (e-mail: k-21760@kepco.co.jp).

The costs of publication of this article were defrayed in part by the payment of page charges. The article must therefore be hereby marked "*advertisement*" in accordance with 18 U.S.C. Section 1734 solely to indicate this fact.

